Impact of Southern California anthropogenic emissions on ozone pollution in the mountain states: Model analysis and observational evidence from space

Min Huang,[1,2] Kevin W. Bowman,[1] Gregory R. Carmichael,[2] R. Bradley Pierce,[3] Helen M. Worden,[4] Ming Luo,[1] Owen R. Cooper,[5,6] Ilana B. Pollack,[5,6] Thomas B. Ryerson,[6] and Steven S. Brown[6]

Received 16 May 2013; revised 23 October 2013; accepted 27 October 2013.

[1] The impact of Southern California (SoCal) anthropogenic emissions on ozone (O_3) in the mountain states in May 2010 is studied using the Sulfur Transport and Deposition Model. We identified two to six major transport events from SoCal to different subregions in the mountain states, with transport times of 0–2 days indicated by trajectories, time-lag correlations, and forward/adjoint sensitivities. Based on forward sensitivity analysis, the contributions from SoCal anthropogenic emissions to the monthly mean daily maximum 8 h average (MDA8) surface O_3 in the mountain states decrease with distance from SoCal, and they range from <1 ppbv (in Wyoming) to 15 ppbv (in western Arizona). These contributions show medium (>0.6) to strong (>0.8) positive correlations with the modeled total surface MDA8 O_3. For the most strongly affected states of Arizona and New Mexico, these contributions have median values of ~3, ~2, ~5, and ~15 ppbv when the total surface MDA8 O_3 exceeded thresholds of 60, 65, 70, and 75 ppbv, respectively. Surface MDA8 O_3 values in SoCal show strong nonlinear responses to varied magnitudes of perturbation (e.g., ±50% and 100%) in SoCal anthropogenic emissions and weak nonlinear responses in the mountain states. Case studies show that different scales of transport (e.g., trans-Pacific, stratospheric intrusions, and interstate) can be dynamically and chemically coupled and simultaneously affect O_3 in the mountain states when the meteorological conditions are favorable. During some of these strong transport periods, the contributions of SoCal anthropogenic emissions to hourly O_3 in the mountain states can exceed 20 ppbv, close to the magnitude during a summer event reported by Langford et al. (2010). Satellite observations from the Tropospheric Emission Spectrometer and the Measurements of Pollution in the Troposphere multispectral retrievals qualitatively demonstrate large and interstate scales of transport, respectively. Suggestions are made for future satellite missions to measure O_3 with improved spatial coverage, temporal frequency, and near-surface sensitivity to provide better observational constraints on interstate pollution transport studies.

Citation: Huang, M., K. W. Bowman, G. R. Carmichael, R. Bradley Pierce, H. M. Worden, M. Luo, O. R. Cooper, I. B. Pollack, T. B. Ryerson, and S. S. Brown (2013), Impact of Southern California anthropogenic emissions on ozone pollution in the mountain states: Model analysis and observational evidence from space, *J. Geophys. Res. Atmos.*, *118*, doi:10.1002/2013JD020205.

1. Introduction

[2] Tropospheric ozone (O_3) impacts human health [*Smith et al.*, 2009], reduces crop yields [*Avnery et al.*, 2011a, 2011b], and has potential long-term effects on forests and natural ecosystems [*Mauzerall and Wang*, 2001]. Ozone in the "mountain states" in the western U.S. is a growing concern. The "mountain states", including Arizona, Colorado, Utah, Nevada, New Mexico, Idaho, Montana, and Wyoming, experienced a population increase of 21.4% from 2000 to 2010 [*U.S. Census Bureau* 2010, 2011]. These states contain 18 out of the 59 national parks in the U.S., which have vulnerable ecosystems and attract a large number of visitors (National Park Service, www.nps.gov, accessed in 2013). The public and ecosystems in these areas are periodically exposed to high O_3 episodes [e.g., *Langford et al.*, 2010; *Lin*

Additional supporting information may be found in the online version of this article.

[1]Jet Propulsion Laboratory, California Institute of Technology, Pasadena, California, USA.
[2]Center for Global and Regional Environmental Research, University of Iowa, Iowa City, Iowa, USA.
[3]NOAA National Environmental Satellite, Data, and Information Services, Madison, Wisconsin, USA.
[4]National Center for Atmospheric Research, Boulder, Colorado, USA.
[5]Cooperative Institute for Research in Environmental Sciences, University of Colorado, Boulder, Colorado, USA.
[6]NOAA Earth System Research Laboratory, Boulder, Colorado, USA.

Corresponding author: M. Huang, Jet Propulsion Laboratory, California Institute of Technology, MS 233-200, 4800 Oak Grove Dr., Pasadena, CA 91109, USA. (min.huang@jpl.nasa.gov)

2169-897X/13/10.1002/2013JD020205

et al., 2012a, 2012b]. Ozone levels in spring and summer have increased since 1990 at some areas, at rates up to ~0.4 ppbv/yr at certain rural sites as reported by *Cooper et al*. [2012]. Several counties in this region are classified as O_3 nonattainment areas under the current National Ambient Air Quality primary O_3 standard (NAAQS) of 75 ppbv, which aimed at protecting the public health and is in the form of the 3 year average of the annual fourth-highest daily maximum 8 h average (MDA8) concentration (The Green Book Nonattainment Areas for Criteria Pollutants, http://www.epa.gov/airquality/greenbook/map8hr_2008.html, accessed in September 2013). However, the U.S. Environmental Protection Agency (EPA) has proposed to lower it to a level within 60–70 ppbv and may also redefine the national O_3 secondary standard (currently the same as the primary standard) in the form of "cumulative peak-weighted index" (W126) within 7–15 ppm h, to protect sensitive vegetation and ecosystems [*U.S. Environmental Protection Agency*, 2010]. Many regions in the mountain states are projected to violate the proposed primary and secondary standards (*McCarthy* [2010, Figure S1] based on 2006–2008 data; Clean Air Status and Trends Network (CASTNET) annual reports, 2004–2011). Therefore, a better understanding and attribution of the sources impacting O_3 in the mountain states is needed in order to develop effective air quality management strategies to comply with the ever-tightening U.S. air quality standards.

[3] There is some evidence that interstate transport of pollution from the Pacific states (i.e., California, Washington, and Oregon) can exacerbate the air quality in the mountain states. For example, aircraft O_3 Light Detection and Ranging (lidar) measurements and trajectory analysis during one event in mid-July 2009 identified that Southern California (SoCal) pollutants were exported by the "mountain chimney effect" [*Lu and Turco*, 1996] and were responsible for the O_3 "spikes" in Utah and Colorado ~48 h later [*Langford et al*., 2010].

[4] In addition to the interstate pollution transport, trans-Pacific transport of pollution and stratospheric intrusion events can impact O_3 over the eastern North Pacific Ocean and the western U.S., possibly resulting in the overall observed increasing O_3 trend and the periodic O_3 episodes [*Task Force on Hemispheric Transport of Air Pollution (TF HTAP)*, 2010; *National Research Council*, 2009; *Cooper et al*., 2010, 2012; *Lin et al*., 2012a, 2012b; *Langford et al*., 2011; *Ambrose et al*., 2011]. These large-scale transport events have been shown to have a larger impact on the O_3 levels in the mountain states than in the Pacific states [*Zhang et al*., 2011; *Lin et al*., 2012a, 2012b]. This region has the highest mean elevation of the 50 U.S. states [*U.S. Geological Survey*, 2001], and the high topography of the Rocky Mountains increases the likelihood of extra-regional plumes influencing the surface O_3 concentrations. The "extra-regional" plumes, which are typically transported in the middle and upper troposphere, are defined as the pollution not affected by recent U.S. emissions.

[5] The prevailing westerly winds in spring and summer bring the extra-regional plumes in the eastern Pacific and upper troposphere/lower stratosphere (UTLS) to the inland western U.S. [*TF HTAP*, 2010; *National Research Council*, 2009]. These meteorological conditions also lead to the regional-scale pollution transport from the Pacific states to the U.S. interior. Consequently, there are potential dynamical and chemical couplings between the interstate transport, intercontinental pollution transport, and stratospheric intrusions. Some studies have reported the mixing of stratospheric O_3 with anthropogenic or biomass burning plumes in other U.S. regions and seasons [e.g., *Parrish et al*., 2000; *Brioude et al*., 2007]. It is also important to understand whether these different scales of pollution transport can occur simultaneously, and how they impact air quality in the mountain states, particularly the NAAQS O_3 exceedances.

[6] Observations from surface monitors, aircraft, and satellites can help disentangle how these processes affect O_3 distributions in the western U.S. Surface, aircraft, and balloon-borne in situ measurements typically have high accuracy but are limited in time and space. Satellite measurements routinely provide broad geographic coverage but have varied spatial/spectral resolution and retrieval sensitivities at different altitudes. Current satellite measurements have demonstrated robustness in capturing strong transport events at large scales [e.g., *Lin et al*., 2012a, 2012b; *Huang et al*., 2013; *Pfister et al*., 2011], especially in capturing the movement of strong extra-regional plumes in the middle and upper troposphere. Recently, studies have sought to improve the near-surface sensitivity of the satellite retrievals for some species, e.g., carbon monoxide (CO) [*Deeter et al*., 2012]. These multispectral products can be beneficial for characterizing near-surface pollution levels and studying interstate transport.

[7] Based on surface observations, SoCal has the highest annual maximum 8 h average O_3 and the highest number of exceedance days among various California air basins (Table S1) in 2010, indicating their worst air quality in the state and its strong potential impacts on the downwind areas. In May 2010, a major multi-institution field campaign was coordinated by the National Oceanic and Atmospheric Administration (NOAA), entitled California Nexus (CalNex): Research at the Nexus of Air Quality and Climate Change [*Ryerson et al*., 2013]. This field experiment was conducted over California and provided extensive measurements of trace gases and particulate matter using a suite of measurement platforms. In this paper, we use the full-chemistry version of the regional scale Sulfur Transport and Deposition Model (STEM) at 12 km × 12 km horizontal resolution to assess the impact of SoCal anthropogenic emissions on air quality in the mountain states in this month. In section 3.1, we evaluate the model performance with surface, aircraft, and ozonesonde measurements. In section 3.2, forward sensitivity analysis is used to estimate the contributions of SoCal (defined in Figure 1a) anthropogenic emissions to surface MDA8 O_3 in the downwind mountain states and the relationship with O_3 exceedances in these areas. The transport times and the frequency of transport events are studied. In addition, the nonlinearity of the source-receptor relationship is discussed to account for a wide range of the possible uncertainties and future changes in SoCal anthropogenic emissions. In section 3.3, we demonstrate that the predicted SoCal O_3 and CO export features are consistent with the observed near-surface CO from Measurements of Pollution in the Troposphere (MOPITT). Case studies in section 3.4 focus on the periods when the transport of Asian and UTLS air masses were coupled with the SoCal anthropogenic pollution export. We use satellite observations to identify the large-scale transport events and forward and adjoint sensitivity analysis to interpret the coupling of different transported plumes. Finally, we summarize the conclusions and their policy-relevant implications and make suggestions for the future observation systems (section 4).

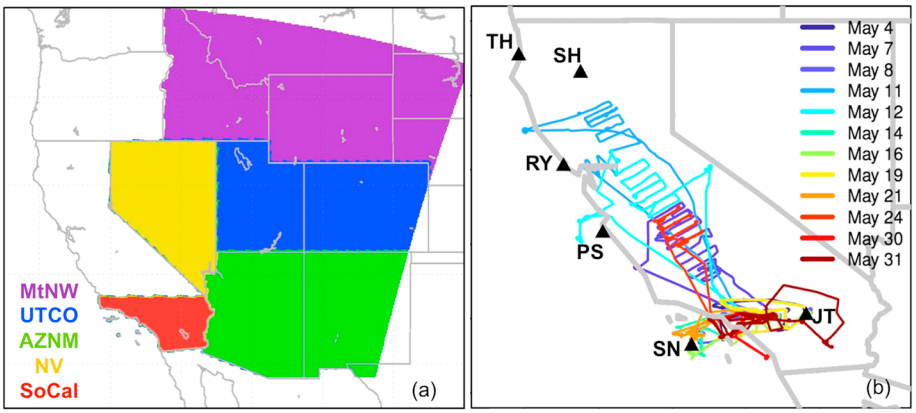

Figure 1. (a) Definition of SoCal and the four mountain subregions used in the discussions. (b) NOAA WP-3D flight paths in May 2010. Flight paths on various days are shown in different line colors. Six black triangles denote the ozonesonde locations.

2. Methods

2.1. Study Period and Meteorological Conditions

[8] The study period is May 2010, during which time the NOAA CalNex field campaign was conducted. *Liang et al.* [2005] concluded that trans-Pacific transport of pollution may be enhanced when there is an enhanced meridional sea level pressure gradient in the North Pacific (stronger North Pacific high and Aleutian low pressure systems) or when higher Pacific/North American (PNA) indexes [*Wallace and Gutzler*, 1981] exist. The gridded (2.5° × 2.5°) NCEP/NCAR reanalysis data [*Kalnay et al.*, 1996] (Figure S2 in the supporting information) show that mean sea level pressure during May 2010 had a stronger meridional gradient in the North Pacific than the 1981–2010 average. The PNA index (900) was slightly higher than the 30 year averages for the month of May (590) but lower than the PNA values in May 2005–2008 (3200–16,600). Therefore, this month represents a period of stronger-than-climatology spring trans-Pacific transport conditions. *Lin et al.* [2012a] have identified a number of trans-Pacific pollution transport episodes during May–June 2010. They found that Asian emissions contributed 8–15 ppbv to daily MDA8 O_3 on days when the observations exceeded 60 ppbv in the western U.S. The 700 hPa geopotential height and wind fields in the eastern Pacific and the western U.S. indicate that the Pacific High had a stronger-than-average pressure gradient from ocean to land this month. Northwesterly winds dominated in California and southwesterly winds crossed Arizona and New Mexico, with the monthly mean wind speed ~1–2 m/s faster than the climatology. Therefore, this month also represents a period of less stagnant conditions that resulted in rapid SoCal pollution export.

[9] The monthly mean tropopause pressure (ranging from ~150 hPa to ~280 hPa in the western U.S.) was up to 40 hPa greater than climatology in the northwestern U.S., whereas the 300 hPa relative humidity (RH) was ~10% lower than the climatology, indicating stronger stratospheric influences on this region. Observations and model-based analyses have reported a number of strong stratospheric intrusion events this May that impacted various regions in the western U.S. [e.g., *Lin et al.*, 2012b; *Neuman et al.*, 2012; *Langford et al.*, 2011].

[10] Previous studies have also concluded that RH and precipitation are negatively correlated with O_3 production while temperature is positively correlated with local O_3 production [*Steiner et al.*, 2006; *Camalier et al.*, 2007]. Lower temperature may lead to weaker secondary production of O_3 in the transported plumes as they travel to the lower altitudes over the western U.S. (e.g., peroxyacyl nitrates (PAN) decomposition [*Fischer et al.*, 2010]). The mean near-surface temperatures in the western U.S. in May 2010 were up to ~5 K lower than the 1981–2010 averages (Figure S2), with larger anomalies in the mountain states. The precipitation in the southwestern U.S. was below normal whereas in the northwestern U.S. it was above normal (National Climate Data Center, accessed in 2013, http://www.ncdc.noaa.gov/sotc/national/2010/5). Therefore, relative to climatology, May 2010 temperatures favored lower local O_3 production and weaker decomposition of PAN transported to the western U.S., while the precipitation favored stronger local O_3 production in the southwestern U.S. and weaker production in the northwestern U.S.

2.2. Observations Used

[11] The observations used in this study include the following:

[12] 1. Surface monitoring networks: Hourly O_3 from U.S. EPA Air Quality System (AQS) and CASTNET sites (Figures 2a and 2b) in May 2010 is used to evaluate the modeled surface O_3.

[13] 2. Aircraft: Ozone, nitrogen oxides (NO_x, nitrogen monoxide (NO), and nitrogen dioxide (NO_2)), and formaldehyde (HCHO) observations collected by the NOAA WP-3D over California are used to evaluate the model performance in the vertical. Ozone and NO_x were measured by two different instruments (i.e., chemiluminescence and cavity ring down spectroscopy). HCHO was measured by proton transfer reaction–mass spectrometry. Ozone and NO_2 measured by the two instruments are highly correlated ($r > 0.9$), with the mean and standard deviations of all used samples differing from each other by <10%, while the two sets of NO measurements show larger differences. Different line colors in Figure 1b denote individual flight paths on 4, 7, 8, 11, 12, 14, 16, 19, 21, 24, 30, and 31 May. The orange solid line in Figure 3a shows the sample sizes at various altitudes. Most of these samples were taken below ~4 km above sea level (asl) over SoCal.

[14] 3. Ozonesondes: Ozonesondes at six California locations spanning ~8° in latitude, starting from ~7 to 10 May with

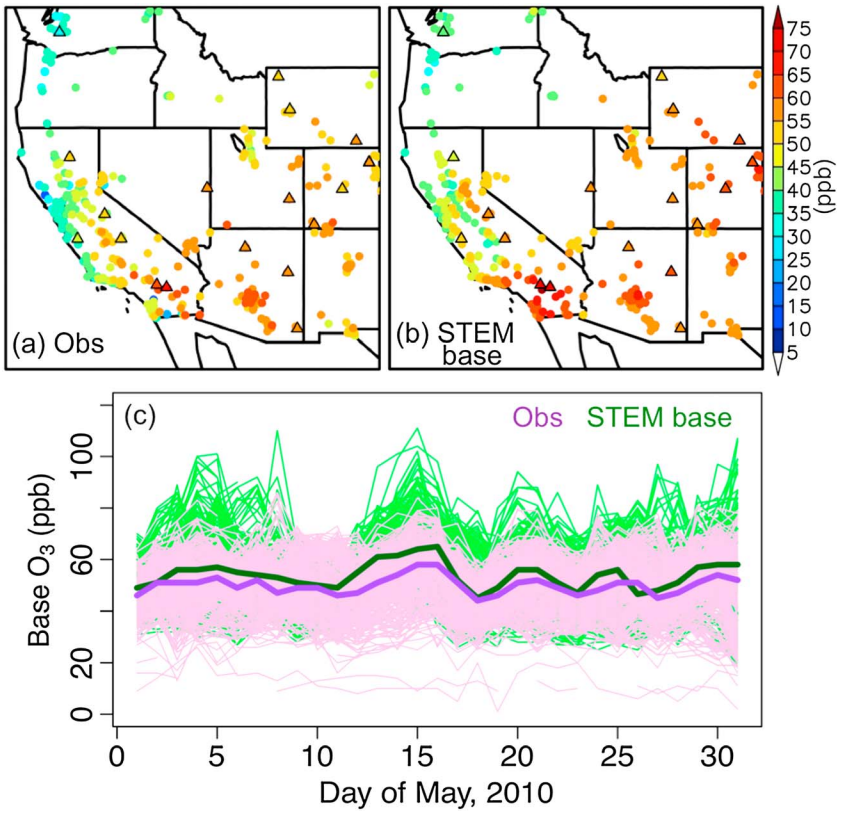

Figure 2. Evaluation of STEM-modeled O_3 at the surface: (a) observed and (b) modeled monthly mean MDA8 O_3 at AQS (circles) and CASTNET (triangles) surface monitoring sites; (c) time series of observed (pink) and modeled (green) MDA8 at individual AQS and CASTNET sites, in thin lines. Thick purple and dark green lines denote the median values at these sites.

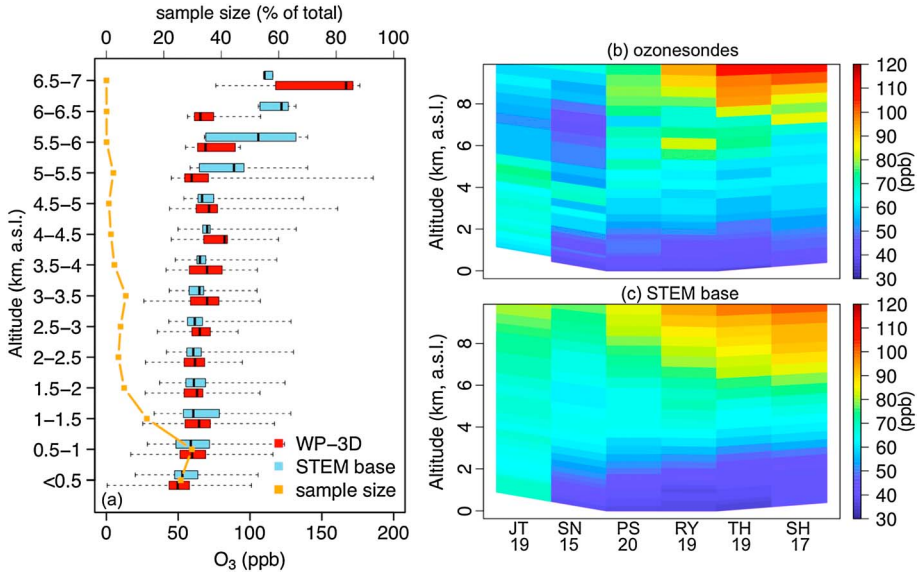

Figure 3. Evaluation of STEM-modeled O_3 in the vertical: (a) box-and-whisker (minimum, 25% percentile, median, 75% percentile, and maximum) plot of the observed and modeled O_3 vertical profiles along all WP-3D flights in May. The data were binned vertically with a 500 m interval, and the sample sizes for each bin are shown in orange. Vertical profiles of monthly median (b) ozonesondes (binned to model vertical layers at each location) and (c) modeled O_3 vertical profiles in May 2010 at six California locations shown in Figure 1b. The numbers below the names of these sites indicate the number of O_3 profiles used at the corresponding locations.

Table 1. Description of the Chemical Measurements Used in This Study[a]

Species	Platform/Network	Methods	Sampling Frequency	Spatial Coverage and Resolution
O_3	AQS and CASTNET at the surface	UV; UV absorption; UV radiation absorption; UV 2B Model 202	hourly	Western U.S.
O_3 and NO_x	NOAA WP-3D	chemiluminescence and cavity ring down spectroscopy from two teams	12 flight days in May	California (mostly SoCal)
HCHO	NOAA WP-3D	proton transfer reaction–mass spectrometry		
O_3	sondes	electrochemical detection methods through the reaction of O_3 in an aqueous potassium iodide solution in an electrochemical cell	close to daily, vary among sites	six locations in California [*Cooper et al*., 2011]
O_3	OMI total column	retrieved from UV backscattered radiation	daily, ~13:40 ascending node equator crossing time	global in 1° × 1°
O_3	TES Level 2 V4 profiles	retrieved from high spectral resolution thermal radiances	7 May, ~13:40 ascending node equator crossing time, in global survey mode	various locations in Eastern Pacific and Western U.S.
O_3	TES Level 3 tropospheric columns and profiles		every other day	global in 2° × 4°
CO	MOPITT V5J NIR/TIR profiles	retrieved from CO absorption in TIR and NIR channels	global coverage every 3 days, ~10:30 am descending node equator crossing time	Western U.S.

[a]Abbreviations: AQS: Air Quality System; CASTNET: Clean Air Status and Trends Network; MOPITT: Measurements of Pollution in the Troposphere; NIR/TIR: near/thermal infrared; OMI: Ozone Monitoring Instrument; TES: Tropospheric Emission Spectrometer; UV: ultraviolet.

a near-daily frequency (varying among sites) [*Cooper et al*., 2011]. Most of these sondes were launched at midafternoon local times. The sites are Shasta (SH), Trinidad Head (TH), Point Reyes (RY), Point Sur (PS), San Nicolas Island (SN), and Joshua Tree National Park (JT), and their locations are shown in Figure 1b as black triangles. These sondes are also used to evaluate the modeled O_3 in the vertical.

[15] 4. Satellite measurements:

a. MOPITT is on board the Earth Observing System (EOS)-Terra satellite and has an ~10:30 A.M. local time descending node equator crossing. The new MOPITT multispectral near/thermal infrared (NIR/TIR) V5J CO profiles are retrieved at 10 levels from "surface" to 100 hPa (i.e., "surface", 900 hPa, 800 hPa, 700 hPa, 600 hPa, 500 hPa, 400 hPa, 300 hPa, 200 hPa, and 100 hPa). When the surface pressure is greater than 900 hPa, the "surface" concentration refers to the mean volume mixing ratio over the layer between the surface and 900 hPa; when the surface pressure is less than 900 hPa, it is the mean volume mixing ratio from the surface to the closest retrieval level above the surface. The multispectral CO retrieval has improved near-surface sensitivity over the inland areas during daytime [*Deeter et al*., 2012], and the comparison of MOPITT CO retrievals in the near-surface layer with in situ aircraft profiles over the continental U.S. indicates a MOPITT high bias of ~3%. This product has recently been used to study urban pollution [*Worden et al*., 2012; *Pommier et al*., 2013], and in this study, we use it to identify the features of SoCal pollution export to the downwind states. We only use the daytime measurements where both the MOPITT cloud detection and the Moderate Resolution Imaging Spectroradiometer (MODIS) cloud mask indicate clear sky conditions.

b. Tropospheric Emission Spectrometer (TES) and Ozone Monitoring Instrument (OMI), both on board the Aura satellite which has an ascending equator crossing time of ~13:40 local time. TES Level 2 (L2) O_3 profiles and Level 3 (L3) O_3 and H_2O data on a 2° × 4° grid were used to identify the large-scale pollution transport features. TES daily L3 data are generated based on its L2 data by Delaunay triangulation followed by 2-D interpolation [*TES Level 3 Algorithms*, *Requirements and Products*, 2005]. TES L2 retrievals do not have the capability of resolving the boundary layer O_3 distribution except in summertime when there is strong thermal contrast between ground and air. The TES O_3 has ~5–20% positive biases over lidar and sonde profiles [*Nassar et al*., 2008; *Richards et al*., 2008; *Boxe et al*., 2010]. Daily total O_3 columns from OMI were used in the online Tropospheric Ultraviolet-Visible (TUV) radiation model [*Madronich et al*., 2002] to generate the photolysis rates for STEM.

[16] The methods, sampling frequency, and spatial coverage for these observations are summarized in Table 1.

2.3. Model and Its Inputs

2.3.1. Model

[17] Model simulations were conducted using the full-chemistry version of the STEM model 2K3, on a 12 km × 12 km Lambert conformal conic grid over the western U.S., with 32 vertical layers in the troposphere (~11 layers below 1 km and ~20–21 layers below 4 km, similar as in *Huang et al*. [2013]). The model calculates gas-phase chemistry reactions based on the SAPRC 99 gaseous chemical mechanism [*Carter*, 2000] with 30 photolysis rates calculated online by the TUV model. It has been used and evaluated in a number of field campaigns in the past decade [e.g., *Carmichael et al*., 2003a, 2003b; *Tang et al*., 2004, 2007; *Adhikary et al*., 2010; *Stith et al*., 2009; *Huang et al*., 2010, 2013]. In this study, STEM base and sensitivity simulations were conducted to generate total O_3 distributions in the western U.S. and to estimate the contributions of SoCal anthropogenic emissions to O_3 in the mountain states.

2.3.2. Meteorology

[18] Meteorology fields were generated by the Advanced Research Weather Research and Forecasting Model (WRF-ARW) [*Skamarock et al*., 2008] version 3.3.1, driven by North American Regional Reanalysis data (32 km horizontal and 3-hourly temporal resolution) [*Mesinger et al*., 2006]. Different landuse data sets and boundary layer (PBL) schemes were tested. There are currently two landuse classifications in WRF, i.e., the 24-category USGS land use (default option) and the 20-category IGBP-modified MODIS. Compared to the USGS data, the MODIS land use data show expanded urban area in SoCal and cropland areas in the Central Valley, whereas the cropland areas shrink in the mountain northwest (Figure S3). The usage of MODIS land use over USGS land use has demonstrated better model performance over urban regions in China [*Yu et al*., 2012] and in some California regions [*Angevine et al*., 2012]. We conducted three WRF simulations using different combinations of the land use and PBL scheme options: (1) USGS land use and Mellor-Yamada-Janjic (MYJ) PBL scheme [*Janjic*, 1994]; (2) MODIS landuse and the Mellor-Yamada-Nakanishi and Niino (MYNN) Level 2.5 PBL scheme [*Nakanishi and Niino*, 2006]; and (3) MODIS land use and MYJ PBL scheme. Urban physics (three-category single-layer urban canopy model with surface effects for roofs, walls, and streets) was included. We compared several simulated meteorological variables (i.e., pressure, temperature, RH, wind speed, and direction) with the observations along all WP-3D flight tracks in May, and planetary boundary layer height (PBLH) at the CalTech supersite since 15 May 2010. The average profiles of temperature, pressure, RH, and wind fields along all WP-3D flight tracks from all three WRF simulations are similar, showing fairly good model performance (Figure S4). The case using MODIS land use generated more stable PBLH at the CalTech supersite (e.g., avoided the unrealistically high PBLH on some days), and usage the of MYNN PBL scheme overall resulted in shallower PBLH, similar to the findings by *Saide et al*. [2011] and *Yver et al*. [2013]. In general, the third simulation that used MODIS land use and MYJ PBL scheme showed the closest simulated PBLH to the observations (Figure S5) and therefore is selected to drive the STEM simulations. The remaining major WRF configurations were the same as those used in *Huang et al*. [2010].

2.3.3. Boundary Conditions

[19] STEM uses time-varying boundary conditions in the lateral and at the model top, downscaled from global model simulations. In this study, the lateral boundary conditions (LBCs) for gaseous and aerosol species and top boundary conditions (TBCs) for 10 gaseous species were downscaled from archived ($1° \times 1°$ horizontal and 6-hourly temporal resolution) Real-Time Air Quality Modeling System (RAQMS) [*Pierce et al*., 2007] global real-time chemical analyses which assimilated the OMI O_3 columns and Microwave Limb Sounder (MLS, also on board the Aura satellite) stratospheric O_3 profiles. The assimilated RAQMS O_3 profiles show fairly good agreement with in situ measurements and ozonesondes in California (i.e., $<$ ±20% mean biases) [*Pierce*, 2011].

[20] The CO boundary conditions from RAQMS in the base and all sensitivity simulations were reduced uniformly by 25 ppbv, because an ~25 ppbv positive bias was estimated based on the comparison of the simulation that used the original RAQMS CO boundary conditions with (1) MOPITT data over the inland western U.S. in May 2010, after applying the MOPITT averaging kernels (MOPITT V4 and V5 Users guide, accessed in 2012, http://www.acd.ucar.edu/mopitt/publications.shtml), and (2) WP-3D aircraft measurements in California. This positive bias is likely due to the RAQMS simulation that scaled up the Asian CO emissions, which is not supported by a recent study that shows a decreasing trend in total CO columns over eastern China of ~1%/yr, based on satellite observations [*Worden et al*., 2013].

2.3.4. Emissions

[21] In the STEM base simulation, anthropogenic emissions were taken from the 2005 National Emissions Inventory (NEI 2005), which varies on weekdays and weekends and includes diurnal cycles. The emissions for CO, NO_x, and volatile organic compounds (VOCs) were scaled by −25%, −20%, and −15%, respectively, based on U.S. EPA emission trends from 2005 to 2010 over the U.S. and the California Air Resources Board (CARB) emission trends over California. The reductions from 2005 to 2010 in the EPA national emission inventory of several other critical primary pollutants (e.g., Particulate Matter (PM) and ammonia (NH_3)) were below 10%, and therefore, their emissions were not scaled in the base simulation. The CO and NO_x emissions over SoCal may still have positive biases after being scaled down, as *Russell et al*. [2012] reported a 30–50% decrease in OMI NO_2 columns over SoCal urban areas. In another study, using a top-down method and flight observations during CalNex, *Brioude et al*. [2013] found CO and NO_x emissions to be 43% and 32% lower than the NEI 2005 values in LA County, respectively, and 37% and 27% lower in the South Coast Air Basin, respectively.

[22] The biogenic emissions were generated by the Model of Emissions of Gases and Aerosols from Nature (MEGAN) [*Guenther et al*., 2006] version 2.04, based on the WRF-calculated temperature and radiation, and the MODIS monthly mean leaf area index data for May 2010.

[23] Daily biomass burning emissions were provided by the high resolution Fire Inventory of National Center for Atmospheric Research (FINN), prepared for the SAPRC 99 chemical mechanism based on MODIS Rapid Response fire counts. This inventory indicates larger biomass and area burnt (for all land types) globally in 2010 than the 2005–2009 mean and generally emits higher CO, Sulfur Dioxide (SO_2), NO, black carbon, and organic carbon and lower non-methane hydrocarbon (NMHC) compared to the Global Fire Emissions Database (GFED) version 3.1 [*Wiedinmyer et al*., 2011]. The total biomass burning emissions were unevenly distributed vertically from the surface to ~1.5–2 km above ground level (agl) with nonlinear factors decreasing from 0.12 to 0.013 as the model altitude increased, same as in *Huang et al*. [2013] and *Adhikary et al*. [2010]. The injection heights were close to the analyzed satellite (i.e., Multiangle Imaging Spectroradiometer (MISR)) wildfire plume injection heights during previous years (2001–2008) over North America.

2.4. Analysis Methods

2.4.1. Forward Sensitivity Analysis

[24] Three forward sensitivity simulations (Cases FW1–FW3 in Table 2) were conducted using the full-chemistry version of STEM to evaluate the impact of SoCal anthropogenic emissions on O_3 in the downwind states. In Case

Table 2. Description of Model Sensitivity Simulations in This Study

Cases	Type of Simulation	Simulated Period	Changes in SoCal Anthropogenic Emissions
FW1	forward sensitivity	May 2010	zero out all species
FW2	forward sensitivity	May 2010	all species reduced by 50%
FW3	forward sensitivity	May 2010	all species increased by 50%
ADJ1	adjoint sensitivity: response function is intermountain surfaces O_3 at 00 UTC on May 10, 2010	8–10 May, case study	same as base case

FW1, the SoCal (red areas in Figure 1a) anthropogenic emissions for all species were zeroed out to estimate their contributions to O_3 in the downwind states. To study the source-receptor relationship of SoCal anthropogenic emissions and the surface O_3 in the western U.S., we conducted simulations FW2 and FW3 in which the SoCal anthropogenic emissions of all species were reduced and increased by 50%, respectively.

2.4.2. Trajectory and Time-Lag Correlation Analysis

[25] We calculated 2 day forward trajectories (based on the WRF wind fields used to drive the chemistry simulations) originating from 3 km asl at San Gabriel Mountains in SoCal at 00 UTC (5 P.M. local daylight time, when the westerly winds dominate and SoCal local O_3 pollution is strong) on each day of the month. The O_3 "mountain chimney effect" may occur around the San Gabriel Mountains area [*Langford et al*., 2010]. The trajectories indicate the downwind areas affected by the anthropogenic pollution transport from SoCal and the corresponding transport times.

[26] Time-lag correlation analysis was also conducted to estimate the transport times and pathways of SoCal anthropogenic pollution to the downwind mountain states. This type of analysis has been applied to study the transport times and pathways of the air masses at the Northern California coastal site at Trinidad Head to several sites in Northern Sacramento Valley [*Huang et al*., 2010; *Parrish et al*., 2010]. We correlate the time series of subregional mean surface MDA8 O_3 over SoCal (base case and SoCal anthropogenic emissions contributions) with the time series of subregional mean surface MDA8 O_3 over four mountain subregions (i.e., MtNW, UTCO, AZNM, and NV, defined in Figure 1a), lagged from 0 to 2 days.

2.4.3. Adjoint Sensitivity Analysis

[27] In addition to the model forward sensitivity studies, which quantified the response of chemical distributions in all grids at future times to the perturbations of model inputs or/and parameters, adjoint sensitivities were also calculated. The distributions of the adjoint variable $\lambda_n(t, x)$ in the entire computational domain, named as "instantaneous areas of influence" [*Sandu et al*., 2005], reflect sensitivities of a defined response function J (e.g., O_3 concentrations at a given receptor at a specific time) to change in chemical distributions of the species n (i.e., C_n) in any of the grids x at earlier time t, as expressed in equation (1):

$$\lambda_n(t,x) = \frac{\partial J}{\partial C_n\,(t,x)} \tag{1}$$

[28] The temporally averaged magnitudes of the adjoint variables are defined as "cones of influence" (COIs) in equation (2), and they can indicate the regions where changes in concentrations of species n during $t = 0$ to $T - 1$ most strongly affect the response function J:

$$\mathrm{COI}_n(x) = \frac{1}{T}\Sigma_{t=0}^{T-1}\lambda_n(t,x) \tag{2}$$

[29] The adjoint analysis can (1) help understand the specific processes that lead to a state of the atmosphere and (2) identify areas where perturbations or uncertainties in the concentration of the chemical species of interest at earlier times will result in significant changes in O_3 levels at the receptor site at a future time. Adjoint sensitivity analysis has been applied in a number of previous studies from global to regional scales for gases and aerosols [e.g., *Kopacz et al*., 2011; *Carmichael et al*., 2008; *Hakami et al*., 2006; *Huang et al*., 2013].

[30] The STEM adjoint sensitivity analysis includes horizontal transport, vertical mixing, and chemistry processes in the calculations [*Sandu et al*., 2005]. One STEM adjoint sensitivity simulation (ADJ1 in Table 2) was conducted to understand the surface O_3 sensitivities at the intermountain regions (i.e., subregions MtNW, UTCO, and AZNM in Figure 1a) with respect to O_3 concentrations backward in time during 8–10 May. These receptor regions were shown by the forward sensitivities to be strongly affected by the SoCal anthropogenic pollution during this period (details in section 3.4.1). This adjoint case study helps interpret the linkages between O_3 at the surface and at upwind locations, either from the upwind states or through the model western boundaries during this period. Intermountain region surface O_3 at 00 UTC on 10 May was chosen to be the response function, and the simulation started from 00 UTC on May 8 and ended at 00 UTC on May 10. The adjoint simulation required the completion of a forward model simulation, which used the same inputs as the other forward simulations.

3. Results and Discussions

3.1. Model Evaluation at the Surface and in the Vertical

3.1.1. Model Evaluation at the Surface

[31] The observed and modeled surface monthly mean MDA8 O_3 concentrations are shown in Figures 2a and 2b at EPA AQS (circles) and CASTNET (triangles) sites. High MDA8 O_3 concentrations (>60 ppbv) are observed in SoCal and most mountain states for this month, and MDA8 O_3 values in the Pacific northwest in this month are below ~50 ppbv. The model overestimates O_3 across the intermountain and coastal regions and underestimates O_3 in California's San Joaquin Valley. The correlation coefficient r, mean bias (bias = modeled-observed), mean error (error = |modeled − observed|), mean fractional bias (fractional bias = 2 × (modeled − observed)/(modeled + observed) × 100%), mean

Table 3. Evaluation of the Monthly-Mean Surface MDA8 O_3 With Observations[a]

Observations	Correlation Coefficient r	Mean Bias (ppbv)	Mean Error (ppbv)	Mean Fractional Bias (%)	Mean Fractional Error (%)	Root-Mean-Square Error (ppbv)
AQS	0.61	4.65	6.29	9.56	12.92	8.64
CASTNET	0.80	3.72	4.40	6.85	8.03	5.82

[a]Abbreviations: AQS: Air Quality System; CASTNET: Clean Air Status and Trends Network. The metrics are defined in section 3.1.

fractional error (fractional error = 2 × |(modeled − observed)/(modeled + observed)| × 100%) (suggested by *Boylan and Russell* [2006]), and root-mean-square error at AQS and CASTNET sites are summarized in Table 3. The better performance at the CASTNET sites than at the AQS sites reflects the fewer number of sites and the weaker influences of local emissions. It also indicates that STEM fairly well represents the overall background conditions in the western U.S. for this period.

[32] Figure 2c shows the time series of observed and modeled MDA8 at all individual AQS and CASTNET sites during this month (pink and green thin lines, respectively). The thick purple and dark green lines represent the median values of observed and modeled MDA8, respectively. Both the observations and models indicate four to five major high O_3 events, and the modeled median MDA O_3 values are generally slightly higher than the observed (<5 ppbv), due to the overprediction at coastal and part of the intermountain regions as indicated in Figures 2a and 2b. The model also captures the temporal variability of O_3, NO_x, and HCHO at the CalTech supersite fairly well since mid-May (Figure S5), with slight overpredictions in NO_2 and HCHO.

[33] The model performance at the surface was also evaluated at AQS and CASTNET sites for the days that observed MDA8 O_3 values exceeded several thresholds of 60, 65, 70, and 75 ppbv. Table 4 summarizes the observed and modeled mean and median MDA8 O_3 during the exceedance periods, indicating the model biases of less than ~5 ppbv.

3.1.2. Model Evaluation in the Vertical

[34] The observed and modeled O_3 along all WP-3D flights in May is compared in a box-and-whisker plot (Figure 3a). Observed O_3 profiles were derived from the measurements taken by two instruments. Where there were measurements from only one instrument, we used them directly. Where there were measurements from both instruments, we calculated the average values of the measurements. Elevated (60–70 ppbv) O_3 mixing ratios are observed at multiple altitudes (~1–2 km and ~4–5 km), indicating the impacts from various sources (e.g., extra-regional, aged local production, and marine air) on the sampled air, as reported by *Neuman et al*. [2012]. The model generally captures well the O_3 vertical structures below 5 km but overpredicts O_3 by ~40 ppbv above that. This overprediction at higher altitudes, based on a much smaller number of samples may be due to the uncertainties in the boundary conditions as well as the coarser model vertical resolution in the free troposphere.

[35] A similar box-and-whisker plot was made only for samples taken in SoCal. Positive biases of less than 10 ppbv for the modeled median and mean O_3 are found for the samples taken below 1 km, consistent with the model evaluation at the surface (Figures 2a and 2b and Table 5). The impact of this positive bias on our conclusions will be further discussed in section 3.2.6. The model also captures the vertical structures of NO_x and HCHO along the all flight tracks (Figure S4) and along SoCal flight tracks fairly well (Table S2). Consistent with the findings at CalTech supersite, we find slight overpredictions in NO_2 and HCHO near the surface in SoCal.

[36] We also compared the monthly median O_3 profiles at six ozonesonde locations in California (Figures 3b and 3c). At each location, the individual ozonesonde profiles on various days were binned to the model vertical layers before calculating the median values. Below 5 km asl, at the inland SoCal site JT, over 60 ppbv of O_3 was observed, indicating the impact of SoCal sources. In contrast, at the other five sonde locations, the lower troposphere was relatively clean (<50 ppbv of O_3), indicating that the impact of U.S. anthropogenic emissions was relatively weaker. In the free troposphere, O_3 enhancements demonstrate latitudinal gradients in the vertical. Polluted air masses and stratospheric intrusions that descend isentropically along the West Coast may explain this feature [*Cooper et al*., 2011]. The model results generally show similar but smoother vertical and latitudinal gradients compared to the sondes, due to the coarser model vertical resolution. At the two SoCal sonde locations (SN and JT) that bracket Los Angeles (LA), the modeled O_3 is reasonably consistent with the sondes below ~3 km (Table 5) but shows up to over 40 ppbv of positive biases in the upper troposphere, possibly introduced from the RAQMS boundary conditions.

3.2. Contributions of SoCal Anthropogenic Emissions to O_3 in the Mountain States

3.2.1. Spatial Distributions of SoCal Contributions

[37] The contribution of SoCal anthropogenic emissions to the monthly mean surface MDA8 O_3 in the downwind mountain states is shown in Figures 4a and 4b, in ppbv and in % of the modeled total O_3, respectively. This contribution was calculated based on the differences between the base case and the forward sensitivity case FW1, which zeroed out all

Table 4. Evaluation of the Surface MDA8 O_3 on O_3 Exceedance Days[a]

	>60 ppbv	>65 ppbv	>70 ppbv	>75 ppbv
Observations (AQS and CASTNET)	65/65	70/68	74/74	78/77
STEM	68/66	72/70	77/75	83/81

[a]Abbreviations: AQS: Air Quality System; CASTNET: Clean Air Status and Trends Network. Mean and median values from observations and the model base simulation are shown.

Table 5. Evaluation of the Modeled O_3 in SoCal at Various Altitudes[a]

	Surface MDA8		<1 km asl			1-3 km asl			≥3 km asl		
	AQS	CASTNET	WP3-D	Sonde (SN)	Sonde (JT)	WP3-D	Sonde (SN)	Sonde (JT)	WP3-D	Sonde (SN)	Sonde (JT)
Observations	49/49	66/66	62/62	44/42	NA	65/65	54/53	63/63	70/71	60/56	68/64
Model	60/58	73/70	69/68	47/42	NA	68/64	56/55	67/67	65/65	67/66	71/69

[a]Abbreviations: AQS: Air Quality System; CASTNET: Clean Air Status and Trends Network. Mean and median values from observations and the model base simulation are shown. Units are ppbv.

anthropogenic emissions in SoCal (Table 2). The largest impact occurs in western Arizona (10–15 ppbv and 15–20% of the total O_3). The impact extends as far as Utah, Colorado, and Wyoming (~1–3 ppbv and ~2–4% of the total).

[38] Using a regional model on a 36 km × 36 km horizontal resolution grid, *Tong and Mauzerall* [2008] concluded that California NO_x emissions were responsible for >18 ppbv of surface MDA8 O_3 in western Arizona, southern Nevada, and southwestern Utah in July 1996, >5 ppbv higher than our estimation. The contributions decreased to ~1–3 ppbv in Colorado and New Mexico, close to the magnitude estimated in this study. The differences between their estimates and ours are mainly due to (1) the decrease in emissions of O_3 precursors and O_3 mixing ratios from 1996 to 2010 in California, (2) the different areas and emission species perturbed, (3) the differences in meteorological conditions, and (4) the differences in model settings (e.g., parameterization and resolution).

3.2.2. SoCal Pollution Transport Pathways and Times

[39] The transport pathways and transport times connecting SoCal and the mountain states during the study period were first investigated using forward trajectories. Figure 4c shows 2 day forward trajectories originating from 3 km asl at the San Gabriel Mountains in SoCal at 5 P.M. local daylight time on each day of the month. Most of these air masses descend into the mountain states, steered by the prevailing southwesterly winds in the southwestern U.S. (Figure S2). The vertical structures of pollution transport along two dominant pathways will be discussed in section 3.3.

[40] The transport time(s) of SoCal anthropogenic pollution to the downwind mountain states were also estimated by time-lag correlation analysis. We correlated the time series of subregional mean surface MDA8 O_3 over SoCal (base case and SoCal anthropogenic emissions contributions) with the time series of subregional mean surface MDA8 O_3 over the four mountain subregions, lagged from 0 to 2 days.

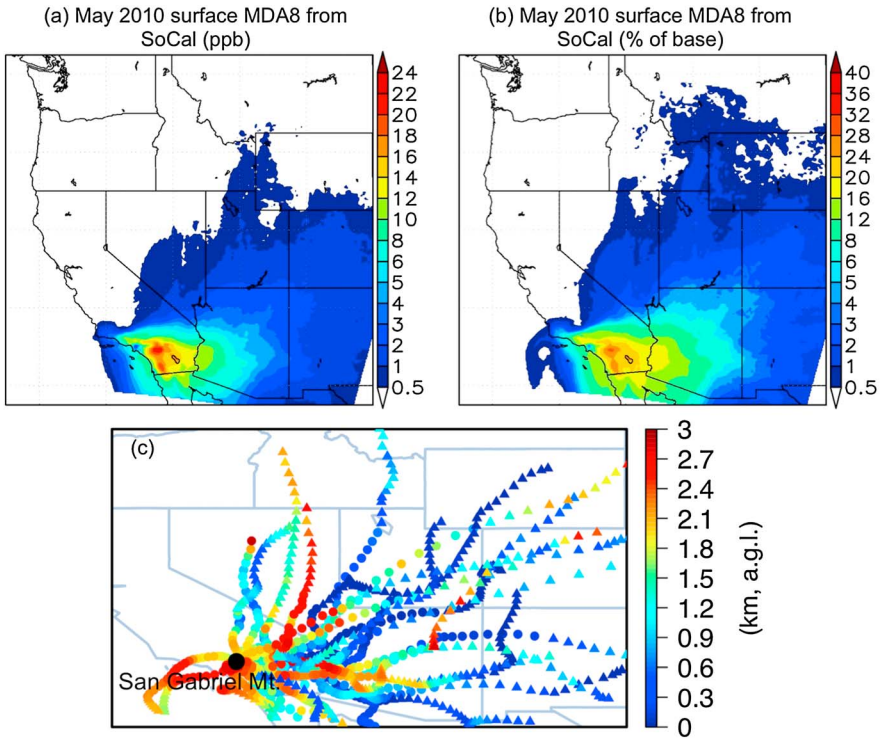

Figure 4. Spatial distributions of the contributions from SoCal anthropogenic emissions: monthly mean SoCal contributions to surface MDA8 O_3 in (a) ppb and (b) % of the base O_3. (c) Two day forward trajectories from San Gabriel Mountain in SoCal (black dot) at 00 UTC of each day in May, based on the 12 km WRF meteorology and they are colored by traveling altitudes (only values smaller than 3 km are shown). Traveling times of <24 h and 24–48 h (after export from SoCal) are denoted by circles and triangles, respectively.

Table 6. Time-Lag Correlations of the Subregional Mean MDA8 O_3 Time Series: Base Case O_3 in SoCal and Base Case O_3 in the Mountain Subregions[a]

Mountain Subregions	0 Day Offset	1 Day Offset	2 Day Offset
MtNW	−0.06	**0.22**	**0.22**
UTCO	0.30	**0.50**	0.11
AZNM	0.52	**0.53**	−0.07
NV	**0.62**	0.50	0.19

[a]The highest correlations for each subregion are in bold. The subregions are defined in Figure 1a.

The results are summarized in Tables 6 and 7. Moderate (>0.6) correlations are found between SoCal O_3 and O_3 in the mountain subregions, with the maxima occurring in AZNM and NV and the minima in MtNW due to the differences in transport distances (the mean distances from San Gabriel Mountains in SoCal to MtNW, UTCO, AZNM, and NV are 1332 km, 965 km, 783 km, and 557 km, respectively) and the predominant westerly wind directions. The transport times are <1 day for NV, ~1 day for UTCO and AZNM, and 1–2 days for MtNW. These estimated transport times, are generally consistent with those based on the trajectory analysis.

3.2.3. Temporal Variability of SoCal Contributions and Its Relationship With Total O_3

[41] Figures 5a–5e show the temporal variability of total surface MDA8 O_3 and the contributions of SoCal anthropogenic emissions to the O_3 variability in the four mountain subregions and SoCal defined in Figure 1a. In each subregion, we plotted the subregional mean daily surface MDA8 O_3 as time series plots from the base simulation (blue lines), showing two to eight major events (strong positive anomalies). The time series of the SoCal anthropogenic emission contributions is shown as red solid lines, indicating two to six major interstate transport events from SoCal to these mountain state subregions, with the contributions ranging from ~1 ppbv (MtNW) to ~9 ppbv (AZNM). The time series of modeled surface MDA8 O_3 in SoCal is also shown (Figure 5e). About two to six episodes are found, and the local anthropogenic emissions contribute up to ~35% to the total MDA8 O_3. The episodes with high contributions from SoCal anthropogenic emissions in SoCal occur 0–2 days earlier than those in the mountain subregions, which is consistent with the findings on transport times in section 3.2.2.

[42] To explore the relationship between surface O_3 levels in the western U.S. and the contributions of SoCal anthropogenic emissions, the correlation coefficient r between the time series of surface MDA8 O_3 from the base simulation and the contributions of SoCal anthropogenic emissions was calculated. This calculation was done in all model grids where the monthly mean SoCal anthropogenic emission contributions were higher than 0.5 ppbv (Figure 5f). Moderate (>0.6) to high (>0.8) r values are shown in Arizona, Colorado, northern New Mexico, and Nevada, and the strongest correlations are found in southern Nevada and western Arizona. The positive correlations in these areas indicate that the contributions of SoCal anthropogenic emissions can exacerbate the air quality problems over these downwind areas, and the uncertainty in SoCal anthropogenic emissions can cause the biases in predicted O_3 in the mountain states. The weak negative correlations in Utah indicate the dominant impacts by other processes such as the transported Asian pollution and stratospheric O_3.

3.2.4. Contributions of SoCal Anthropogenic Emissions on O_3 Exceedance Days

[43] To further quantify the relationship between the O_3 exceedances and the contributions from SoCal anthropogenic emissions, we calculated the monthly mean SoCal contributions to MDA8 O_3 in each model grid on all of the days in May and only on the days that O_3 exceeded several thresholds (current and proposed NAAQS primary O_3 standards) for that grid.

[44] The number of days in May that the modeled total O_3 exceeded current or potential MDA8 thresholds (i.e., 60, 65, 70, 75 ppbv) for all of the model grids belonging to each of the four mountain subregions (Figure 1a) is calculated and shown in Figure 6a as a box-and-whisker plot. The span and the median number of days exceeding the different thresholds in each subregion decrease as the threshold value increases. This plot is qualitatively consistent with our knowledge that O_3 exceedances in these regions are marginal under the current national primary O_3 standard [e.g., *Ling*, 2012], but indicates that an expanded area in the mountain states will have O_3 exceedances if the national primary O_3 standard is tightened.

[45] Contributions of SoCal anthropogenic emissions to surface MDA8 O_3 in the mountain states are shown in Figure 6b also as a box-and-whisker plot for the days exceeding these various thresholds. Again, the highest contributions occur in AZNM, and the magnitudes of SoCal contributions are generally positively correlated to the thresholds, e.g., the median SoCal contributions to surface MDA8 O_3 in AZNM on all days, and days total MDA8 O_3 that exceeded 60, 65, 70, and 75 ppbv are ~2, ~3, ~2, ~5, and ~15 ppbv, respectively. The finding is generally consistent with the correlation map (Figure 5f).

3.2.5. The Nonlinearity of Source-Receptor Relationship

[46] To study the effect of the magnitudes of the perturbation in SoCal anthropogenic emissions on the corresponding changes in surface MDA8 O_3 levels in the western U.S., we conducted two forward sensitivity simulations in which the SoCal anthropogenic emissions for all species were decreased and increased by 50%, respectively (cases FW2 and FW3, defined in Table 2). The extent of nonlinearity in the responses was evaluated using the dimensionless metrics "Scale 1" and "Scale 2":

$$\text{Scale 1} = (\text{base case } O_3 - \text{case FW2 } O_3) \times 2/(\text{base case } O_3 - \text{case FW1 } O_3) \quad (3)$$

$$\text{Scale 2} = (\text{case FW3 } O_3 - \text{base case } O_3) \times 2/(\text{base case } O_3 - \text{case FW1 } O_3) \quad (4)$$

Table 7. Time-Lag Correlations of the Subregional Mean MDA8 O_3 Time Series: SoCal Anthropogenic Emissions Contributions to SoCal O_3 and Base Case O_3 in the Mountain Subregions[a]

Mountain Subregions	0 Day Offset	1 Day Offset	2 Day Offset
MtNW	0.24	**0.42**	0.25
UTCO	0.38	**0.47**	0.09
AZNM	**0.50**	0.48	−0.11
NV	**0.57**	0.44	0.14

[a]The highest correlations for each subregion are in bold. The subregions are defined in Figure 1a.

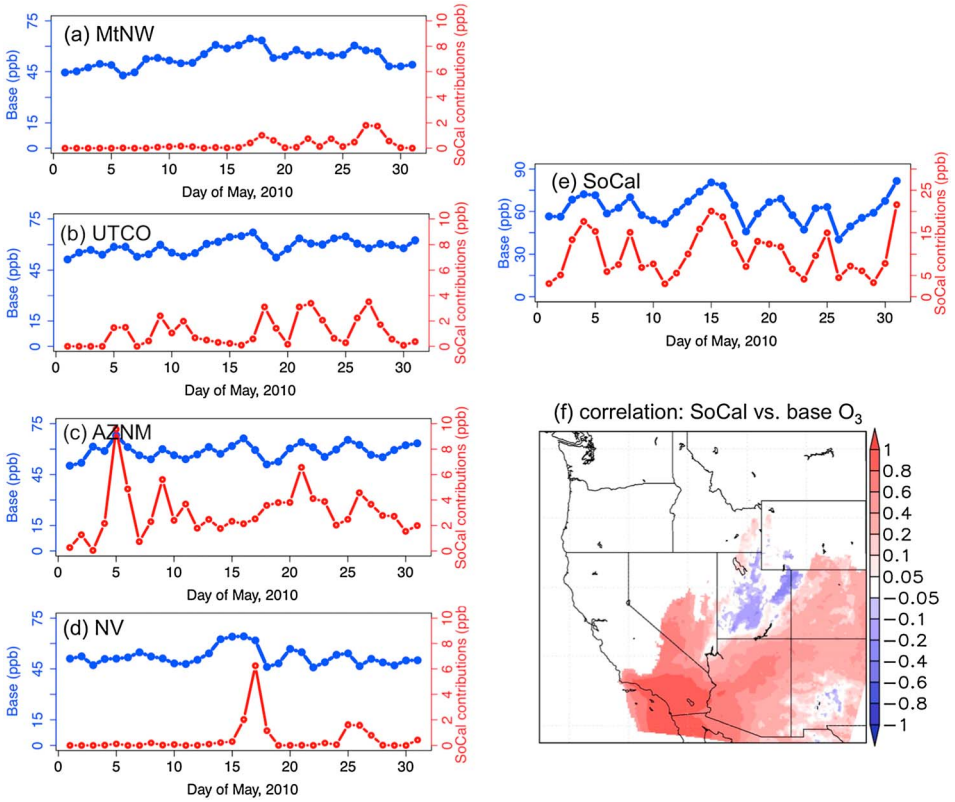

Figure 5. Temporal variability of the contributions from SoCal anthropogenic emissions: time series of modeled subregional mean surface MDA8 base O_3 (blue lines) and the SoCal contributions to O_3 in four mountain subregions (a) MtNW, (b) UTCO, (c) AZNM, and (d) NV and in (e) SoCal. (f) Correlation coefficients r between the time series of modeled surface MDA8 O_3 and the SoCal contributions. They were only calculated for the grids that SoCal contributions to the surface monthly mean MDA8 O_3 were larger than 0.5 ppb.

[47] The Scale 1 metric represents nonlinearity of surface MDA8 O_3 responses when scaling the original SoCal anthropogenic emissions by a number within the range of 0–1. The Scale 2 metric indicates the nonlinearity when scaling the original SoCal anthropogenic emissions by factors larger than 1. Closer-to-1 values for both of them indicate weaker nonlinearity. The metrics reflect the "scalability" of estimated contributions from SoCal anthropogenic emissions, i.e., if we have O_3 sensitivity (at both source and receptor sides) to a specific perturbation in emissions, how accurate the sensitivities to other magnitudes of the emission perturbations would be based on linear interpolation or extrapolation.

[48] We calculate these two metrics using the surface MDA8 O_3 from the different simulations (in the model grids where SoCal anthropogenic emissions contributed >0.5 ppbv to the monthly mean surface MDA8 O_3). The spatial distributions of Scale 1 and Scale 2 in the western U.S. are shown in Figures 7a and 7b, respectively, and Figure 7c depicts the two metrics as a function of distance from San Gabriel Mountains in SoCal. These figures show that Scale 1 values are closer to 1 than those of Scale 2, indicating weaker nonlinear MDA8 O_3 source-receptor relationship when scaling the original SoCal anthropogenic emissions by a number in the range of 0–1 than a number larger than 1. Strongest nonlinearity occurs in SoCal reflected by both metrics. A few negative values are shown <100 km from San Gabriel Mountains (Figure 7c), which may be due to the chemical

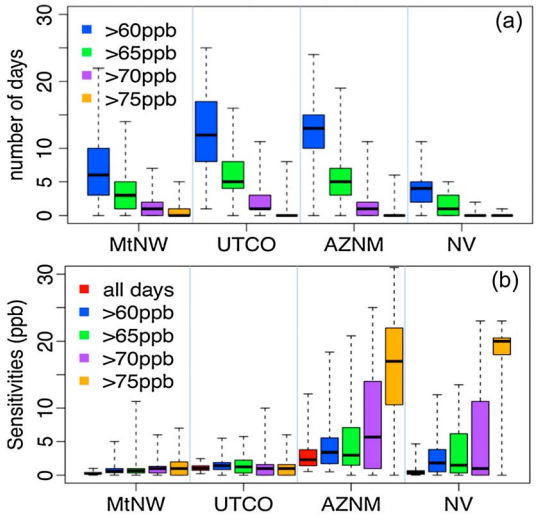

Figure 6. Contributions of SoCal anthropogenic emissions to O_3 exceedances in the mountain states: box-and-whisker plots (minimum, 25% percentile, median, 75% percentile, and maximum) of (a) the number of days of O_3 exceedance in May, based on current and proposed primary O_3 standards (60 ppbv, 65 ppbv, 70 ppbv, and 75 ppbv) in the four mountain subregions. (b) SoCal contributions to the monthly-mean surface MDA8 O_3 calculated on all days and on the O_3 exceeding days in May 2010.

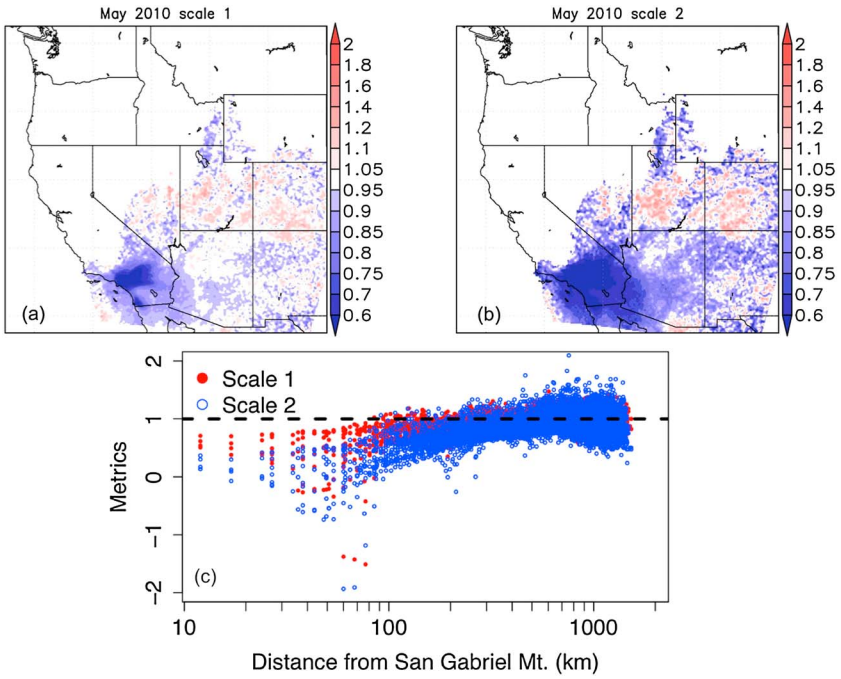

Figure 7. Nonlinearity of O_3 responses to different magnitudes of perturbation in SoCal anthropogenic emissions: monthly mean (a) Scale 1 and (b) Scale 2 at the surface. They are defined in section 3.2.5 and indicate the extents of nonlinearity. (c) Scale 1 and Scale 2 as a function of distance from the San Gabriel Mountain area in SoCal.

regimes (e.g., strong VOC limited in LA urban area in contrast to NO_x limited and transitional in the surrounding rural areas [*Duncan et al*., 2010]). The metrics relax back to unity (~1) at ~300–500 km away from the San Gabriel Mountains. The fluctuations of these metrics reflect the effects of topography in the mountain states and the complex local chemistry.

[49] The subregional mean of Scale 1 and Scale 2 values is closer to 1 over the four mountain subregions than over SoCal (Table 8). Among the four mountain subregions, the weakest nonlinearity occurs in UTCO, and the strongest nonlinearity occurs in AZNM. *Fiore et al*. [2009] and *Wild et al*. [2012] studied the responses of North American and European surface O_3 to perturbations in European NO_x emissions. They found that the nonlinear relationship varied among seasons, and the overall extent of the nonlinearity in Europe (the source) was larger than in NA (the receptor). This is qualitatively consistent with our findings.

[50] The discussions in this section were based on three sensitivity simulations in which the emissions of all species were perturbed. In future work, a larger number of sensitivity simulations with varied perturbations on different precursor species can help better shape the nonlinear response curve.

3.2.6. Uncertainty Discussions

[51] Figures 2a, 2b, and 3a and Table 5 indicate that the model base simulation overpredicts ~11 ppbv (+22% of total) and ~7 ppbv (+11% of total) for O_3 at the surface sites and along the flight tracks at altitudes below 1 km in SoCal, respectively. This overall positive bias can be introduced from multiple factors such as boundary conditions, meteorology, chemical mechanism, deposition, and local anthropogenic and non-anthropogenic emissions. We assume that all of these factors equally contributed to the 10%–22% positive biases in the predicted near-surface O_3 in SoCal. Based on the source-receptor relationship found in section 3.2.5 (i.e., Scale 1 of 0.75 in SoCal in Table 8), a reduction in 11%–22% of SoCal O_3 contributed from its local anthropogenic pollution can be achieved by a 15%–30% reduction in the used SoCal anthropogenic emissions. This amount of reduction in anthropogenic emissions may lead to a 15%–30% decrease in the estimated SoCal contributions to O_3 in the mountain states, based on the Scale 1 values of 0.95–1 in the mountain states (Table 8). Future work on better attributing the model biases to different factors will be needed to improve the bias analysis.

3.3. Interstate Pollution Transport Indicated by MOPITT CO

[52] Representing pollution transport on smaller scales (e.g., interstate) using satellite O_3 data remains a challenge as the existing satellite O_3 profiles do not have strong near-surface sensitivity [*Martin*, 2008; *Bowman*, 2013]. Here we explore the capability of multispectral MOPITT CO products to capture the features of interstate transport of pollution from SoCal, and whether these transport features indicated by MOPITT are consistent with the modeled SoCal anthropogenic CO and O_3 export.

[53] Figure 8a shows the daytime (~17–20 UTC overpass time in the model domain) "surface" CO from the MOPITT NIR/TIR V5J product for the entire month, binned to a

Table 8. Subregional Mean Scale 1 and Scale 2 Metrics[a]

Metrics	MtNW	UTCO	AZNM	NV	SoCal
Scale 1	0.95	~1.00	0.96	0.99	0.75
Scale 2	0.86	0.99	0.89	0.91	0.46

[a]The metrics are defined in section 3.2.5.

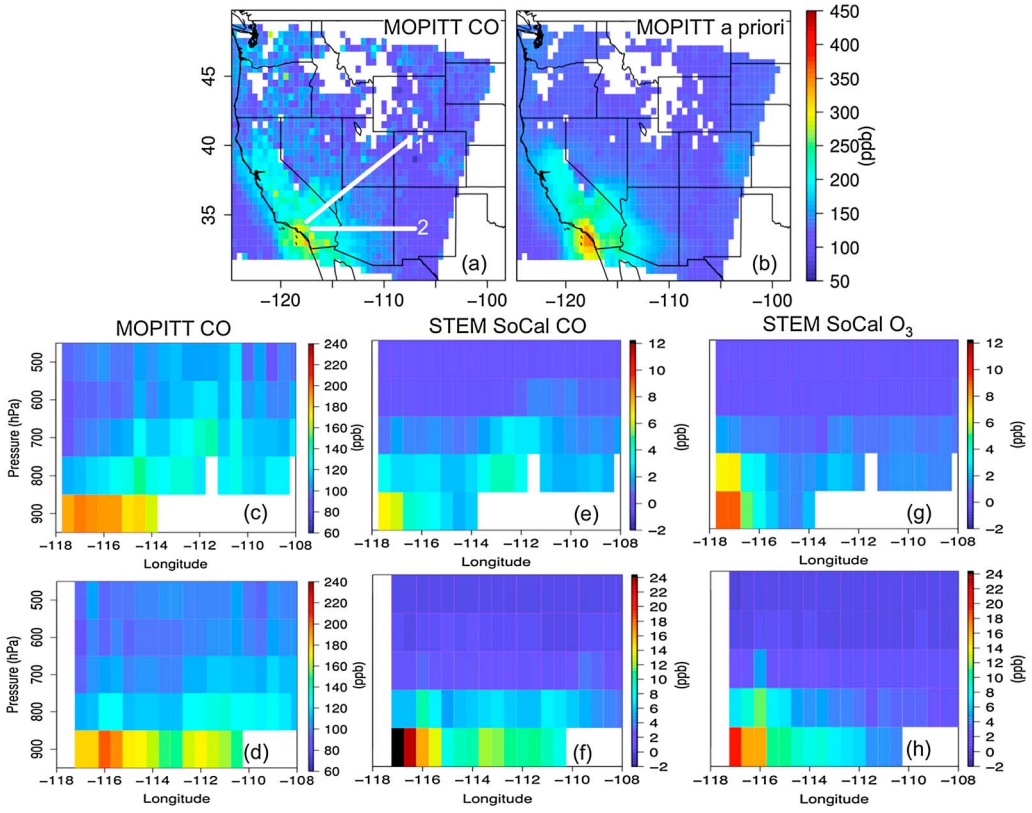

Figure 8. (a) MOPITT NIR/TIR V5J daytime "surface" CO in May 2010 and (b) its a priori, gridded to 0.5°×0.5°. (c, d) MOPITT daytime CO along two dominant transport cross sections 1 and 2. The cross sections are denoted as white solid lines in Figure 8a. STEM-modeled SoCal contributions to monthly mean (e, f) 19 UTC CO and (g, h) 00 UTC O_3 along cross sections 1 and 2.

$0.5° \times 0.5°$ grid. Over 200 ppbv of CO is observed in California, western Arizona, southern Nevada, and the urban regions in Washington and Oregon, with the highest magnitude shown in SoCal (>300 ppbv). These MOPITT CO retrievals show significant differences (e.g., >50 ppbv less in SoCal) from their a priori (Figure 8b). The mean and standard deviation of the degree of freedom for signal (DOFS, trace of the diagonals of the averaging kernel) for MOPITT inland samples located in the studied domains are 1.61 and 0.24, respectively. The differences between MOPITT retrievals and their a priori, together with the DOFS, show that MOPITT observations have fairly good sensitivity to near-surface CO. After applying the MOPITT averaging kernels, the STEM-modeled surface CO spatial pattern is similar to MOPITT, with the correlation coefficient *r*, mean bias, mean error, mean fractional bias, mean fractional error, and root-mean-square error of 0.89, 2.75 ppb, 11.68 ppb, 2.60%, 8.10%, and 16.16 ppb, respectively.

[54] The monthly mean daytime MOPITT CO (gridded to 0.5° interval in longitude) mixing ratios along two cross sections are shown in Figures 8c and 8d, respectively. Cross section 1 extends from the San Gabriel Mountains to southern Nevada/Utah/Colorado, and cross section 2 extends from the San Bernardino Mountains to Arizona. Both cross sections are denoted as thick white lines in Figure 8a. These cross sections are selected to represent the dominant pathways that SoCal air masses travel toward the mountain states, as indicated by the forward trajectories in Figure 4c. High CO mixing ratios are observed in eastern LA near the surface (>180 ppbv), indicating the strong local contribution from SoCal anthropogenic emissions sources. Elevated CO concentrations (>120 ppbv) are observed by MOPITT from the "surface" to ~700 hPa at ~114–110°W along both cross sections.

[55] The modeled monthly mean SoCal anthropogenic emissions contributions to CO at 19 UTC (close to MOPITT overpass times in SoCal) are shown along these two cross sections in Figures 8e and 8f in MOPITT vertical grids, respectively, indicating that SoCal anthropogenic emissions strongly affect local CO levels and contribute ~6 ppbv and ~16 ppbv of CO (in maximum) in Utah and Arizona, respectively, decreasing from the surface to ~500–600 hPa. While the gradients in the original vertical grids are smoothed after the regridding, the vertical structure is preserved. The modeled monthly mean SoCal anthropogenic emissions contributions to O_3 at 00 UTC are also shown along these two cross sections in Figures 8 g and 8 h in the MOPITT vertical grids, respectively, showing similar spatial patterns as for CO. The maximum SoCal anthropogenic emissions contributions to O_3 in Utah and Arizona are ~4 ppbv and ~12 ppbv, respectively.

[56] The consistency between the vertical gradients of MOPITT CO and modeled contributions of SoCal anthropogenic emissions to CO and O_3 indicates that the current multispectral satellite product with improved near-surface sensitivity can provide some useful information on the interstate pollution transport.

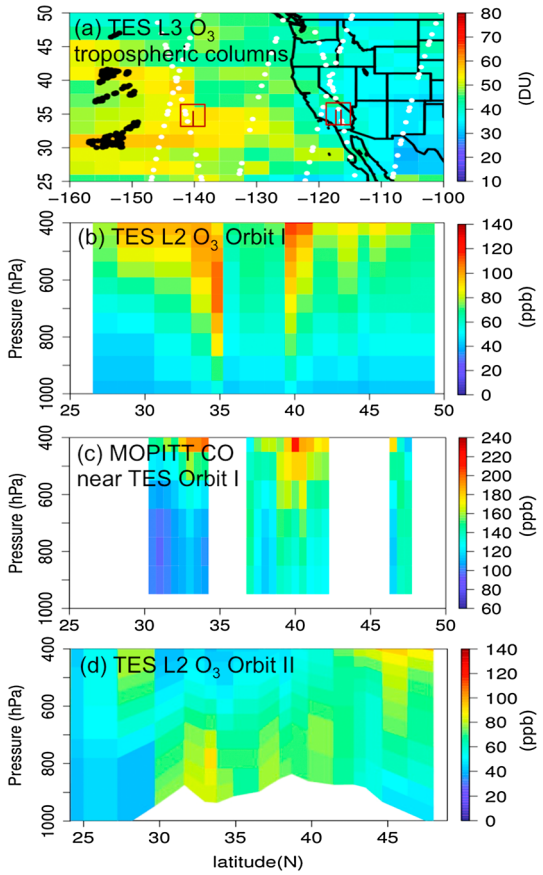

Figure 9. Satellite detecting impacts of extra-regional pollution: (a) TES L3 products (in 2°×4° grids) tropospheric O_3 columns in DU (1 DU = 2.69×10^{16} molecules/cm^2) on 7–8 May. The actual TES orbits filtered by the quality flag and C-curve are overlaid as white dots. TES L2 data along the orbits (b) I and (d) II, observed at ~23 UTC and ~21 UTC on 7 May, respectively (denoted in the dark red text boxes in Figure 9a). (c) MOPITT NIR/TIR V5J CO profiles in the Pacific, averaged latitudinally with a 0.5° interval. These sample locations are shown as black dots in Figure 9a. Note that MOPITT V5J uses only TIR radiances over the ocean, with good sensitivity to the mid- troposphere.

3.4. Concurrent Transport

3.4.1. SoCal Pollution Export Coupled With Trans-Pacific Transport of Asian Pollution

[57] *Lin et al.* [2012a] found that trans-Pacific transport of pollution impacted the western U.S. during 8–10 May, and these Asian-origin air masses were sampled by WP-3D over SoCal [*Neuman et al.*, 2012]. In this section we study in detail how Asian and SoCal pollution simultaneously affected O_3 levels in the mountain states during this period.

[58] The capability of satellites to capture trans-Pacific transport of pollution is investigated first. Figure 9a shows TES L3 tropospheric O_3 columns for 7–8 May. On 7–8 May, >50 Dobson units (DU) of tropospheric O_3 columns were observed in broad areas of the eastern North Pacific and western U.S. coastal regions, ~5–10 DU higher than the monthly mean values, indicating strong influence from extra-regional sources. The O_3 vertical distributions along TES ascending orbits I and II (noted in Figure 9a, red text boxes) are shown in Figures 9b and 9d, respectively. Orbit I was sampled at ~23 UTC on 7 May in the eastern Pacific, and >80 ppbv of O_3 was observed above ~800 hPa around 35°N and 40°N. At ~20–21 UTC on this day, MOPITT measured enhanced CO in the middle troposphere in the Pacific, near TES Orbit I (black dots in Figure 9a). The enhanced CO concentrations are also shown at ~35°N and 40°N (Figure 9c), similar latitudes to the high TES O_3, and indicate that the extra-regional plumes may be mainly from anthropogenic or biomass burning emission sources. At about the same hour, TES passed across Pacific states (along Orbit II), and ~60–80 ppbv of O_3 was observed over broad regions below ~600 hPa at 30–45°N, indicating the impact of extra-regional O_3 that descended to the Pacific states (Figure 9d). An O_3 hot spot (~100 ppbv) was observed at ~800 hPa in SoCal at ~33°N, which may indicate the addition of SoCal anthropogenic pollution to the enhanced O_3 background. This profile had strong retrieval sensitivity based on the comparison with its a priori and the examination of its averaging kernel matrix. In Figure S6, we show the profiles of this retrieval and its a priori, together with the diagonal of its averaging kernel matrix. This profile's DOFS values are >1.4 and >0.5 in the troposphere and at near-surface (> ~750 hPa), respectively. STEM also simulates elevated O_3 levels near TES Orbit II but shows an overall negative bias after applying the TES observation operator in a range of ~ −37 to ~16 ppbv from the surface to ~400 hPa, with mean/median biases of ~ −10 ppbv. This is mainly due to the uncertainties in the boundary conditions.

[59] Using satellite measurements of total CO columns from Atmospheric Infrared Sounder (AIRS) and model sensitivity analysis, *Lin et al.* [2012a] have shown that trans-Pacific transport of pollution from Asia started to impact California on 7 May. We also conducted forward sensitivity simulations in which O_3 in the boundary conditions was reduced by 50% (Text S1). Surface O_3 in the intermountain region during 7–10 May shows stronger sensitivities than the monthly averages to this perturbation in the boundary conditions during 7–10 May, indicating anomalous impacts from extra-regional plumes (not shown). These stronger sensitivities occurred in regions that were found by *Lin et al.* [2012a] to also have been affected by Asian emissions. SoCal local production can be another important contributor to the O_3 hot spot observed by TES in SoCal (Figure 9c). The topography of the two major mountain ranges in eastern LA (the San Gabriel and San Bernardino Mountains) is >1.5 km (Figure 10a). The MODIS land use database (used in the STEM simulation, pink triangles) shows mostly urban areas in LA county, southwest of these two mountain ranges. A cross section (red line in Figure 10a) is made connecting the coastal areas with the San Gabriel Mountains, transecting the similar general region studied by *Langford et al.* [2010]. Modeled total O_3 along the cross section at 00 UTC on 8 May (5 P.M. local time, close to TES overpass time in SoCal) is shown in Figure 10b, with black solid lines and dotted lines denoting the WRF-modeled PBLH (increases from <500 m at the coastal areas to >1 km inland) and the topography, respectively. Two disconnected layers of high O_3 are shown: (1) 80–100 ppbv at <2 km asl, south of ~34.2°N, and (2) 80–110 ppbv at ~2–4 km asl, lifted by the San Gabriel Mountains. This vertical structure is qualitatively similar to the lidar-based findings at similar locations in SoCal by *Langford et al.* [2010] and *Lu and Turco*

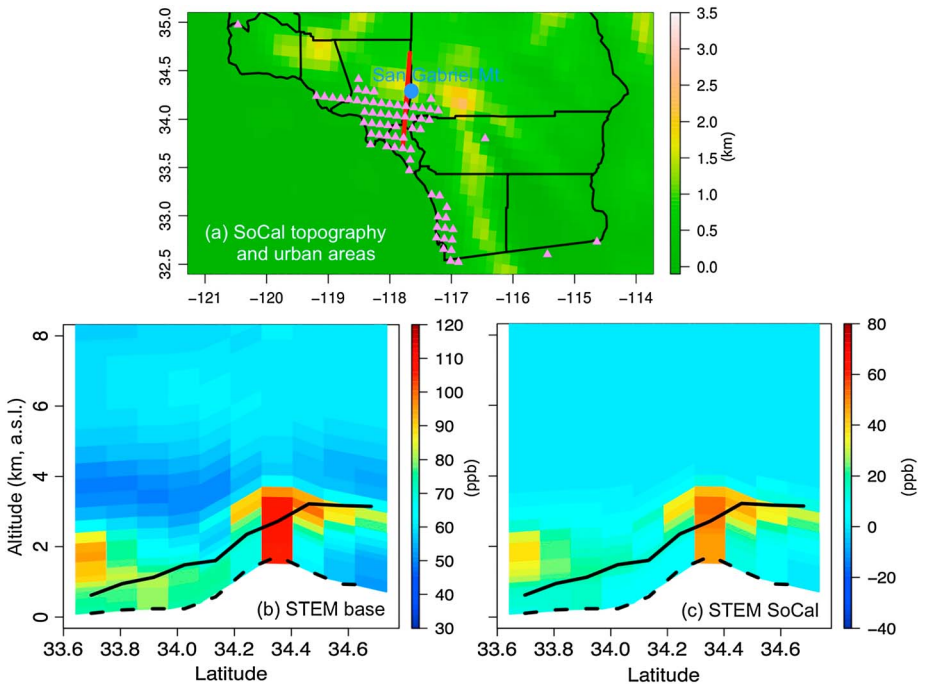

Figure 10. Simulated ozone export from SoCal: (a) the topography over SoCal and urban areas (pink triangles) defined in the simulations. The light blue dot shows San Gabriel Mountain area. (b) STEM base O_3 and (c) SoCal anthropogenic emission contributions to O_3 along the cross section (red solid line in Figure 10a) at 00 UTC on 8 May. The black solid and dotted lines reflect WRF-predicted PBLH and the topography, respectively.

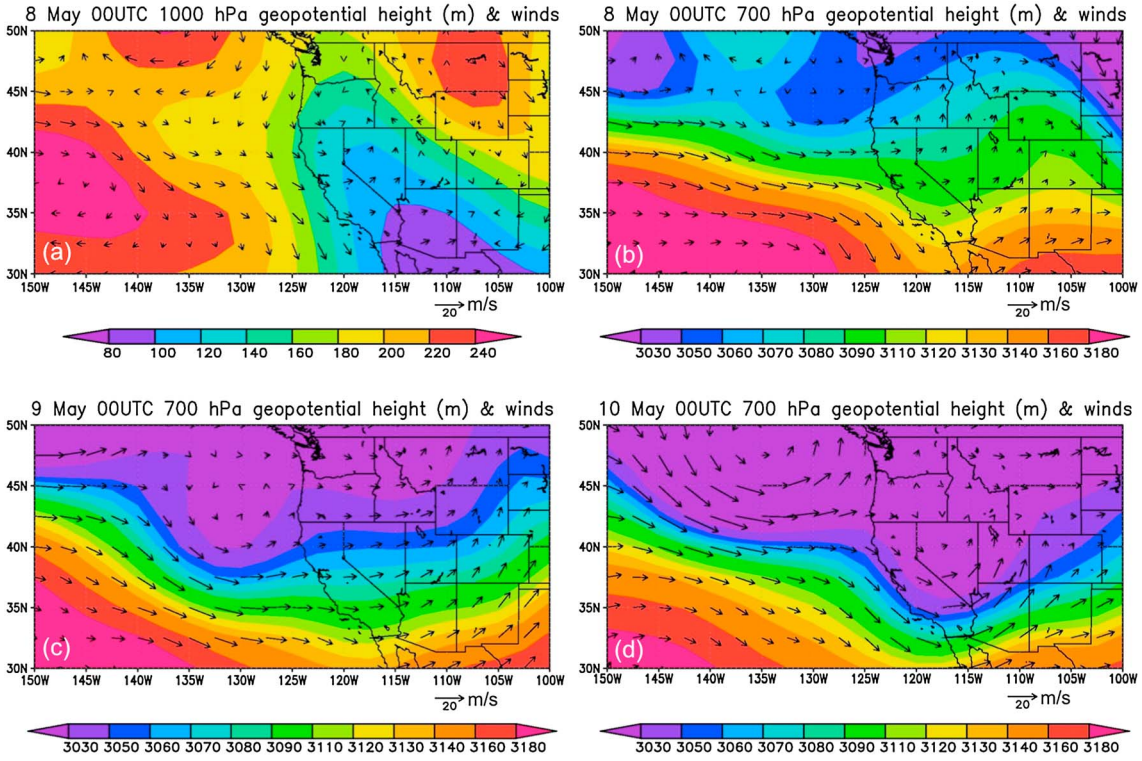

Figure 11. Meteorological conditions during the case study period in section 3.4.1, based on NCAR/NCEP reanalysis data [*Kalnay et al.*, 1996]: (a) 1000 hPa and (b) 700 hPa geopotential height with winds at 00 UTC on 8 May; 700 hPa geopotential height with winds at 00 UTC on (c) 9 May and (d) 10 May.

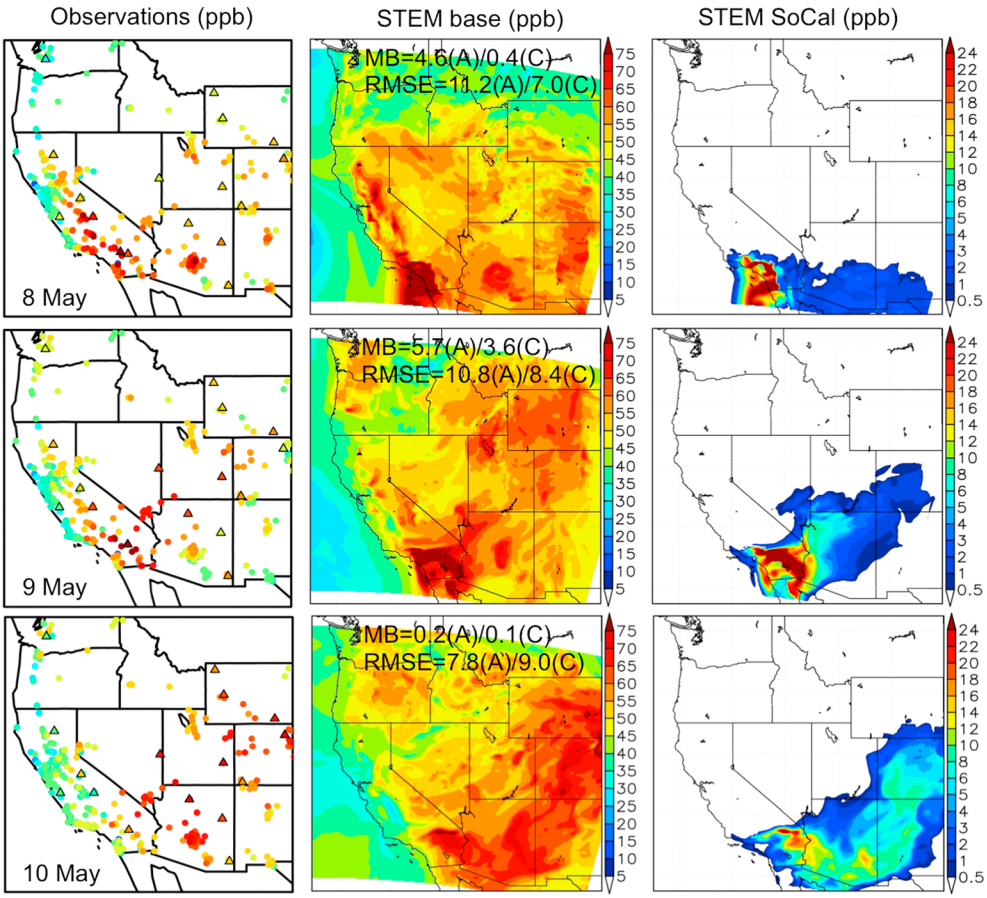

Figure 12. Impact of SoCal anthropogenic emissions on western U.S. surface O_3 at 00 UTC on (first to third rows) 8–10 May: (left column) observed O_3 at the AQS (circles) and CASTNET (triangles) surface sites, (middle column) STEM-modeled base O_3 at the surface, and (right column) the modeled surface O_3 contributed from SoCal anthropogenic emissions. The mean bias (MB) and root-mean-square error (RMSE) in ppb were calculated at AQS (A) and CASTNET (C) sites at the corresponding times and included in the middle column.

[1996], and the magnitude is similar to the TES observation in SoCal at ~800 hPa (Figure 9d) on this day. The model indicates that 80–90 ppbv of this O_3 is exported downwind, similar to the July 2009 case study by *Langford et al.* [2010]. Forward sensitivities indicate that SoCal anthropogenic emissions contribute up to 50% of the total O_3 along this cross section at this time and result in the multilayer O_3 structures in the total O_3 (Figure 10c).

[60] Meteorological conditions since 8 May favor the coupled transport of extra-regional plumes and SoCal anthropogenic pollutants. The surface conditions show high pressure in the eastern Pacific and low pressure extending from Mexico to the southwestern U.S. due to surface heating (Figure 11a). This is similar to the situations discussed in *Langford et al.* [2010] and *Lu and Turco* [1996]. At 700 hPa, unlike the situation in *Langford et al.* [2010] and *Lu and Turco* [1996], a sharper longitudinal gradient of geopotential height is shown in the Pacific. A strong jet (wind speed >20 m/s) is found at 37–40°N, which rotates toward the south and decelerates after reaching the U.S. It shifts southwesterly when passing SoCal and continues to travel toward the mountain states (Figure 11b). This condition is close to the monthly mean spatial pattern (Figure S2), but with enhanced intensity.

[61] The impacts of SoCal anthropogenic emissions on downwind surface O_3 during 8–10 May were further studied. In Figure 12, the left column shows the observations from AQS and CASTNET sites at 00 UTC (5–6 P.M. local daylight times in the studied areas) on 8, 9, and 10 May (first to third rows) as circles and triangles, respectively. The modeled surface O_3 values over the western U.S. at the corresponding times are shown in the middle column. At the times shown, California's Bay Area and the northern Central Valley are relatively clean (surface O_3 <60 ppbv). The model overpredicts O_3 on 8 May and well captures O_3 distributions on the following 2 days over these areas. SoCal O_3 levels are high on 8 and 9 May (>80 ppbv) and drop significantly on 10 May. Overall, the model well captures the O_3 distributions, except the overprediction near San Diego on 8–9 May. Outside of California, >60 ppbv of surface O_3 is observed and modeled on 9 May in the Seattle/Portland urban areas (>50–60 ppbv) due to local emissions/production, and the hot spots moved eastward on the following day. Over 70 ppbv of O_3 is observed and modeled in several mountain states (Utah, Colorado, Arizona, and Wyoming), with generally greater O_3 mixing ratios on 10 May (>70 ppbv).

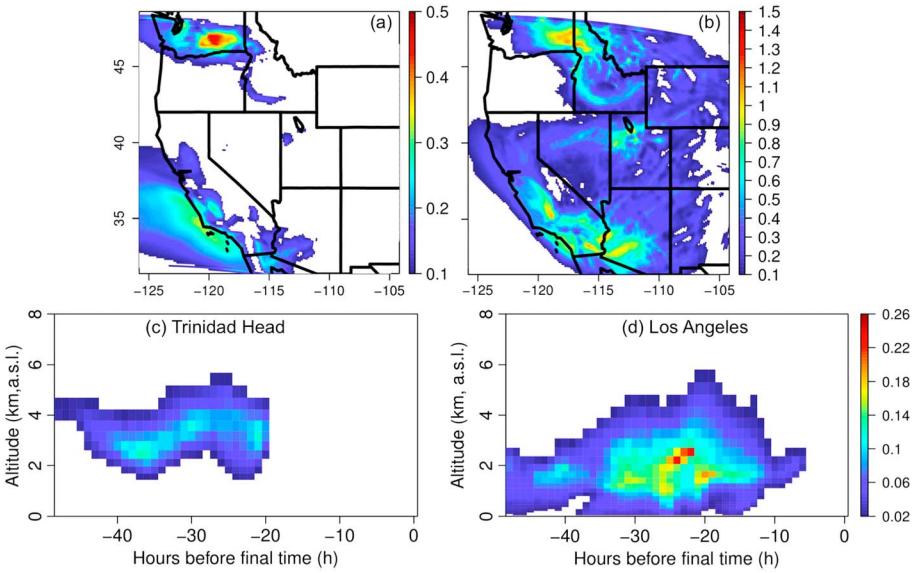

Figure 13. Adjoint sensitivities during the case study period in section 3.4.1: COIs integrated at model levels (a) above ~2 km agl and (b) below ~2 km agl. The time-height curtain plot of $\lambda[O_3]$ at (c) Trinidad Head in Northern California and (d) Los Angeles in SoCal.

[62] We also show the contributions of SoCal anthropogenic emissions to surface O_3 in the right column in Figure 12 at 00 UTC on 8, 9, and 10 May, based on the forward sensitivity calculations. At 00 UTC on 8 May, SoCal anthropogenic emissions contributed <5 ppbv of MDA8 in southern Arizona and New Mexico. On the second day (9 May), the westerly winds crossed California and Arizona with increased speed (affected by the same jet as on 8 May, Figure 11c), and the impacts of SoCal pollution extended to broad areas across Arizona (>10 ppbv of MDA8 O_3 in northwestern Arizona). On the third day (10 May), the southwesterly winds across SoCal remained strong (Figure 11d), and the SoCal pollution was transported as far as Colorado and the impacts covered almost the entire Arizona and New Mexico. The instantaneous impacts in some areas of Arizona were >20 ppbv, resulting in the high total O_3 values there. This magnitude is close to that estimated by *Langford et al.* [2010] during a July 2009 episode.

[63] We calculated adjoint sensitivities to surface O_3 in the intermountain regions to further explore the impacts of transport and subsidence of air masses on surface O_3 in these receptor regions (Case ADJ1 in Table 2). The intermountain states were shown in Figure 11 to be strongly impacted by SoCal anthropogenic emissions. The O_3 adjoint sensitivities ($\lambda[O_3]$) were calculated 49 h backward in time from 00 UTC on 10 May, and the COIs (equation (2)) were calculated by temporally averaging $\lambda[O_3]$ in each model grid over the 2 day period. We further vertically integrated the COIs at the model layers above (Figure 13a) and below (Figure 13b) ~2 km agl. The hot spots of COIs show that intermountain surface O_3 at the end of the simulation was sensitive to middle to lower tropospheric (below ~2 km agl) O_3 in Washington, coastal SoCal, and offshore of the Bay Area, reflecting the impact of extra-regional pollution transport. The final-time intermountain surface O_3 mixing ratios were also most sensitive to near-surface (below ~2 km agl) O_3 in Washington and central and Southern California during the previous 2 days, which indicates the impact of interstate pollution transport from these upwind areas.

[64] Figure 13c shows the time-height curtain plot of $\lambda[O_3]$ at the Trinidad Head grid box in coastal Northern California (Figure 1b) throughout the adjoint simulation period. This site is considered to be strategically located to characterize air masses entering the western U.S. [*Oltmans et al.*, 2008], and enhanced O_3 mixing ratios are typically usually observed aloft there when extra-regional plumes are transported into the region and impact the surface O_3 inland at later times. The high adjoint sensitivities ~20–48 h prior to the final time at ~2–5 km indicate that the extra-regional pollution observed by TES affected surface O_3 concentrations in the intermountain states ~1–2 days later. This figure is consistent with our knowledge that current satellite O_3 profiles that have fairly good sensitivity to O_3 in the middle to lower troposphere can sample the hemispheric-scale pollution transport.

[65] Figure 13d shows the time-height curtain plot of $\lambda[O_3]$ in the LA grid box, an important source of interstate pollution transport, during the adjoint simulation period. High adjoint sensitivities during ~10–48 h prior to the final time at both free troposphere and boundary layer indicate the concurrent transport of local and extra-regional O_3 impacted O_3 in the mountain states and the range of interstate transport time of 0.5–2 days. This figure also emphasizes the need for future satellite products to have the enhanced sensitivity to near-surface O_3 in order to capture the features of interstate O_3 transport.

[66] The satellite observations and model sensitivities during this period show that different scales of transport can simultaneously enhance the surface O_3 levels in the mountain states. Figures 5b and 5c show that during this 3 day period the subregional mean SoCal anthropogenic emissions contributions to UTCO and AZNM surface MDA8 O_3 have maxima of ~3 ppbv and ~6 ppbv, respectively. This magnitude of SoCal anthropogenic emission contribution (by ~22 million people) is close to (but slightly lower than)

the contribution estimated by *Lin et al*. [2012a] from East Asian (>1.5 billion people) pollution for the same time period. This comparison illustrates how a relatively small but nearby pollution source can impact a receptor region almost as efficiently as a much larger source that has been diluted over greater transport distances. Therefore, in addition to improving the estimation of Asian emissions and their contributions, controlling regional anthropogenic emissions (in SoCal and other Pacific states) can help improve the air quality in the mountain states.

3.4.2. SoCal Pollution Export Coupled With Stratospheric Intrusions

[67] *Lin et al*. [2012b] reported a number of strong stratospheric intrusion events during May–June 2010, and their contributions to surface MDA8 O_3 were estimated to be ~20–40 ppbv, ~2–3 times higher than previously reported. Many of these large-scale transport events were also captured by TES observations (Figure S7 shows the spatial plots of L3 TES O_3 and H_2O in the upper troposphere (i.e., 316 hPa)). The intrusion periods (e.g., ~17–19 May, ~23–24 May, and ~27–28 May) were characterized by high O_3 and low H_2O (and also low CO, not shown) in the eastern Pacific and the western U.S. The stratospheric intrusion events during 3–5 May and 11–13 May were also indicated by TES measurements, but the impacts were relatively limited in space across the western U.S. (not shown). RAQMS tropopause pressure (not shown) also shows strong anomalies at the locations where the intrusions occurred as indicated by TES, and due to the uncertainties in RAQMS in UTLS, STEM-modeled O_3 generally shows negative biases at UTLS.

[68] In earlier sections, our forward sensitivity analysis has shown anomalous contributions of SoCal anthropogenic emissions to MDA8 O_3 in the mountain states during these reported stratospheric-impacted periods (Figures 5a–5d), with the contributions to subregional mean MDA8 O_3 ranging from ~1–2 ppbv to >8 ppbv. These magnitudes are significantly smaller than the contributions of 20–40 ppbv from the stratospheric intrusion estimated by *Lin et al*. [2012a].

4. Conclusions and Implications for Future Work

[69] The impact of SoCal anthropogenic emissions on air quality in the mountain states in May 2010 was studied using the full-chemistry version of STEM. For this month, there were two to six major transport events from SoCal to different subregions in the mountain states, with transport times of 0–2 days estimated by trajectory analysis, time-lag correlations, and forward/adjoint sensitivities. The contributions of SoCal anthropogenic emissions to monthly mean surface MDA8 O_3 generally decreased with the distance from SoCal but still contributed >1 ppbv as far as Wyoming. The strongest impact occurred in Arizona and New Mexico, and the median contributions of SoCal anthropogenic emissions to the surface MDA8 O_3 were ~3, ~2, ~5, and ~15 ppbv when their total surface MDA8 O_3 exceeded the thresholds of 60, 65, 70, and 75 ppbv, respectively. These estimated contributions had uncertainties of 15–30%, based on a simple bias correction.

[70] These results have important policy-relevant implications, because the number of days with O_3 exceedances will increase as the O_3 standards become lower. Stronger local emission control efforts may have to be implemented in the mountain states to attain these newer standards, and a better understanding of the contributions from nonlocal sources will also be necessary. Previous studies concluded that the transport of Asian pollution can exacerbate air quality over the mountain states. This study shows that trans-boundary and interstate transport of pollution can concur, and the transport of SoCal anthropogenic pollution contributed similar magnitudes of O_3 in the mountain states as the Asian emission sources. The positive correlation between the contributions of SoCal anthropogenic emissions and the total surface O_3 concentrations in the mountain regions, along with the model estimated SoCal anthropogenic emission contributions on O_3 exceedance days, indicate strong connection between SoCal anthropogenic pollution and the air quality in the mountain states, especially in Arizona, New Mexico, and Nevada. Therefore, controlling emissions in SoCal is expected to improve the air quality in both California and the mountain states. The reduction in the uncertainty in SoCal emissions would also improve the predicted O_3 in both regions and may benefit from the improved future observation system that could be used to constrain the modeling results.

[71] Satellite observations were used to qualitatively provide evidence for different scales of transport in this study. TES detected O_3 aloft over the eastern North Pacific and SoCal, reflecting strong stratospheric intrusions, trans-Pacific transport episodes, and elevated O_3 levels in SoCal. The MOPITT multispectral CO product with improved sensitivity near the surface captured the features of smaller-scale pollution transport and indicated the role of topography for the transport. Careful validation of this new product over extended time and spatial scales will increase confidence in its usage for improving model input fields (such as fine-resolution emissions and boundary conditions) as well as the estimated contributions from interstate transport. In recent years, great efforts have been taken to also improve the near-surface sensitivity of O_3 retrievals [*Worden et al*., 2007; *Fu et al*., 2013; *Cuesta et al*., 2013]. The further development of this technique could be beneficial for directly characterizing near-surface O_3 levels and for further studying smaller-scale transport events. Future geostationary satellites (such as GEO-CAPE, http://geo-cape.larc.nasa.gov) will provide trace gas and PM observations at higher spatial resolution on hourly time scales. These products are expected to be useful for improved understanding of the simultaneous impacts from different scales of transport and for evaluating and improving the model estimates.

[72] **Acknowledgments.** This work was initiated at the University of Iowa and supported by a NASA award NNX11AI52G. It was then continued at Jet Propulsion Laboratory, California Institute of Technology, under a contract with NASA, and was supported by the NASA Aura project. The authors would like to thank the editors and three anonymous reviewers for their efforts on earlier drafts of the paper. We thank the CalNex science team (especially Carsten Warneke for HCHO aircraft measurements and Jochen Stutz, Barry Lefer, Rebecca Washenfelder, and Bernhard Rappenglueck for their measurements at CalTech supersite) and the people who made the AQS, CASTNET, MOPITT and TES measurements. We thank C. Wiedinmyer and T. Duhl (NCAR) for helping with the MEGAN model and FINN data. We also thank computational resources at the University of Iowa and at NASA Ames. The views, opinions, and findings contained in this paper are those of the authors and should not be construed as an official NOAA or U.S. Government position, policy, or decision.

References

Adhikary, B., et al. (2010), A regional scale modeling analysis of aerosol and trace gas distributions over the eastern Pacific during the INTEX-B field campaign, *Atmos. Chem. Phys.*, *10*, 2091–2115, doi:10.5194/acp-10-2091-2010.

Ambrose, J., D. Reidmiller, and D. Jaffe (2011), Causes of high O_3 in the lower free troposphere over the Pacific Northwest as seen at the Mt. Bachelor Observatory, *Atmos. Environ.*, *45*(30), 5302–5315, doi:10.1016/j.atmosenv.2011.06.056.

Angevine, W. M., L. Eddington, K. Durkee, C. Fairall, L. Bianco, and J. Brioude (2012), Meteorological model evaluation for CalNex 2010, *Mon. Weather Rev.*, *140*, 3885–3906.

Avnery, S., D. L. Mauzerall, J. Liu, and L. W. Horowitz (2011a), Global crop yield reductions due to surface ozone exposure: 1. Year 2000 crop production losses and economic damage, *Atmos. Environ.*, *45*, 2284–2296.

Avnery, S., D. L. Mauzerall, J. Liu, and L. W. Horowitz (2011b), Global crop yield reductions due to surface ozone exposure: 2. Year 2030 potential crop production losses and economic damage under two scenarios of O_3 pollution, *Atmos. Environ.*, *45*, 2297–2309.

Bowman, K. W. (2013), Toward the next generation air quality monitoring, ozone, *Atmos. Environ.*, doi:10.1016/j.atmosenv.2013.07.007.

Boxe, C. S., et al. (2010), Validation of northern latitude Tropospheric Emission Spectrometer stare ozone profiles with ARC-IONS sondes during ARCTAS: Sensitivity, bias and error analysis, *Atmos. Chem. Phys.*, *10*, 9901–9914, doi:10.5194/acp-10-9901-2010.

Boylan, J. W., and A. G. Russell (2006), PM and light extinction model performance metrics, goals, and criteria for three-dimensional air quality models, *Atmos. Environ.*, *40*(26), 4946–4959, doi:10.1016/j.atmosenv.2005.09.087.

Brioude, J., et al. (2007), Mixing between a stratospheric intrusion and a biomass burning plume, *Atmos. Chem. Phys.*, *7*, 4229–4235, doi:10.5194/acp-7-4229-2007.

Brioude, J., et al. (2013), Top-down estimate of surface flux in the Los Angeles Basin using a mesoscale inverse modeling technique: Assessing anthropogenic emissions of CO, NO_x and CO_2 and their impacts, *Atmos. Chem. Phys.*, *13*, 3661–3677, doi:10.5194/acp-13-3661-2013.

Camalier, L., W. Cox, and P. Dolwick (2007), The effects of meteorology on ozone in urban areas and their use in assessing ozone trends, *Atmos. Environ.*, *41*, 7127–7137.

Carmichael, G. R., et al. (2003a), Evaluating regional emission estimates using the TRACE-P observations, *J. Geophys. Res.*, *108*(D21), 8810, doi:10.1029/2002JD003116.

Carmichael, G. R., et al. (2003b), Regional-scale chemical transport modeling in support of the analysis of observations obtained during the TRACE-P experiment, *J. Geophys. Res.*, *108*(D21), 8823, doi:10.1029/2002JD003117.

Carmichael, G. R., A. Sandu, T. Chai, D. N. Daescu, E. M. Constantinescu, and Y. Tang (2008), Predicting air quality: Improvements through advanced methods to integrate models and measurements, *J. Comput. Phys.*, *227*, 3540–3571, doi:10.1016/j.jcp.2007.02.024.

Carter, W. P. L. (2000), Documentation of the SAPRC-99 chemical mechanism for VOC reactivity assessment, Final Report to California Air Resources Board, Contract No. 92-329 and 95-308.

Cooper, O. R., et al. (2010), Increasing springtime ozone mixing ratios in the free troposphere over western North America, *Nature*, *463*, doi:10.1038/nature08708.

Cooper, O. R., et al. (2011), Measurement of western U.S. baseline ozone from the surface to the tropopause and assessment of downwind impact regions, *J. Geophys. Res.*, *116*, D00V03, doi:10.1029/2011JD016095.

Cooper, O. R., R. S. Gao, D. W. Tarasick, T. Leblanc, and C. Sweeney (2012), Long-term ozone trends at rural ozone monitoring sites across the United States, 1990–2010, *J. Geophys. Res.*, *117*, D22307, doi:10.1029/2012JD018261.

Cuesta, J., et al. (2013), Satellite observation of lowermost tropospheric ozone by multispectral synergism of IASI thermal infrared and GOME-2 ultraviolet measurements, *Atmos. Chem. Phys. Discuss.*, *13*, 2955–2995, doi:10.5194/acpd-13-2955-2013.

Deeter, M. N., H. M. Worden, D. P. Edwards, J. C. Gille, and A. E. Andrews (2012), Evaluation of MOPITT retrievals of lower tropospheric carbon monoxide over the United States, *J. Geophys. Res.*, *117*, D13306, doi:10.1029/2012JD017553.

Duncan, B. N., et al. (2010), Application of OMI observations to a space-based indicator of NO_x and VOC controls on surface ozone formation, *Atmos. Environ.*, *44*(18), 2213–2223, doi:10.1016/j.atmosenv.2010.03.010.

Fiore, A. M., et al. (2009), Multimodel estimates of intercontinental source receptor relationships for ozone pollution, *J. Geophys. Res.*, *114*, D04301, doi:10.1029/2008JD010816.

Fischer, E. V., D. A. Jaffe, D. R. Reidmiller, and L. Jaegle´ (2010), Meteorological controls on observed peroxyacetyl nitrate at Mount Bachelor during the spring of 2008, *J. Geophys. Res.*, *115*, D03302, doi:10.1029/2009JD012776.

Fu, D., J. R. Worden, X. Liu, S. S. Kulawik, K. W. Bowman, and V. Natraj (2013), Characterization of ozone profiles derived from Aura TES and OMI radiances, *Atmos. Chem. Phys.*, *13*, 3445–3462, doi:10.5194/acp-13-3445-2013.

Guenther, A., T. Karl, P. Harley, C. Wiedinmyer, P. I. Palmer, and C. Geron (2006), Estimates of global terrestrial isoprene emissions using MEGAN (Model of Emissions of Gases and Aerosols from Nature), *Atmos. Chem. Phys.*, *6*, 3181–3210, doi:10.5194/acp-6-3181-2006.

Hakami, A., J. H. Seinfeld, T. F. Chai, Y. H. Tang, G. R. Carmichael, and A. Sandu (2006), Adjoint sensitivity analysis of ozone nonattainment over the continental United States, *Environ. Sci. Tech.*, *40*(12), 3855–3864, doi:10.1021/es052135g.

Huang, M., et al. (2010), Impacts of transported background ozone on California air quality during the ARCTAS-CARB period—A multi-scale modeling study, *Atmos. Chem. Phys.*, *10*, 6947–6968, doi:10.5194/acp-10-6947-2010.

Huang, M., et al. (2013), Impacts of transported background pollutants on summertime western U.S. air quality: Model evaluation, sensitivity analysis and data assimilation, *Atmos. Chem. Phys.*, *13*, 359–391, doi:10.5194/acp-13-359-2013.

Janjic, Z. I. (1994), The Step–Mountain Eta coordinate model: Further developments of the convection, viscous sublayer and turbulence closure schemes, *Mon. Weather Rev.*, *122*, 927–945.

Kalnay, E., et al. (1996), The NCEP/NCAR 40-Year Reanalysis Project, *Bull. Am. Meteorol. Soc.*, *77*, 437–471.

Kopacz, M., D. L. Mauzerall, J. Wang, E. M. Leibensperger, D. K. Henze, and K. Singh (2011), Origin and radiative forcing of black carbon transported to the Himalayas and Tibetan Plateau, *Atmos. Chem. Phys.*, *11*, 2837–2852, doi:10.5194/acp-11-2837-2011.

Langford, A. O., C. J. Senff, R. J. Alvarez II, R. M. Banta, and R. M. Hardesty (2010), Long-range transport of ozone from the Los Angeles Basin: A case study, *Geophys. Res. Lett.*, *37*, L06807, doi:10.1029/2010GL042507.

Langford, A. O., J. Brioude, O. R. Cooper, C. J. Senff, R. J. Alvarez II, R. M. Hardesty, B. J. Johnson, and S. J. Oltmans (2011), Stratospheric influence on surface ozone in the Los Angeles area during late spring and early summer of 2010, *J. Geophys. Res.*, *117*, D00V06, doi:10.1029/2011JD016766.

Liang, Q., L. Jaegle´, and J. M. Wallace (2005), Meteorological indices for Asian outflow and transpacific transport on daily to interannual timescales, *J. Geophys. Res.*, *110*, D18308, doi:10.1029/2005JD005788.

Lin, M., et al. (2012a), Transport of Asian ozone pollution into surface air over the western United States in spring, *J. Geophys. Res.*, *117*, D00V07, doi:10.1029/2011JD016961.

Lin, M., A. Fiore, O. R. R. Cooper, L. W. Horowitz, A. O. O. Langford, H. Levy II, B. J. Johnson, V. Naik, S. J. Oltmans, and C. J. Senff (2012b), Springtime high surface ozone events over the western United States: Quantifying the role of stratospheric intrusions, *J. Geophys. Res.*, *117*, D00V22, doi:10.1029/2012JD018151.

Ling, M. (2012), The Clean Air Act and Transported Air Pollution, WESTAR/UNR Conference on Western Ozone Transport, http://www.westar.org/12%20Tech%20Conf/Presentations/Ling.pdf.

Lu, R., and R. P. Turco (1996), Ozone distributions over the Los Angeles Basin: Three dimensional simulations with the SMOG model, *Atmos. Environ.*, *30*, 4155–4176, doi:10.1016/1352-2310(96)00153-7.

Madronich, S., S. Flocke, J. Zeng, I. Petropavlovskikh, and J. Lee-Taylor (2002), The tropospheric ultra-violet visible (TUV) model manual.

Martin, R. V. (2008), Satellite remote sensing of surface air quality, *Atmos. Environ.*, doi:10.1016/j.atmosenv.2008.07.018.

Mauzerall, D. L., and X. Wang (2001), Protecting agricultural crops from the effects of tropospheric ozone exposure: Reconciling science and standard setting in the United States, Europe and Asia, *Annu. Rev. Energy Environ.*, *26*, 237–268.

McCarthy, J. E. (2010), Ozone Air Quality Standards: EPA's Proposed January 2010 Revision, http://www.fas.org/sgp/crs/misc/R41062.pdf.

Mesinger, F., et al. (2006), North American regional reanalysis, *Bull. Am. Meteorol. Soc.*, *87*(3), 343–360, doi:10.1175/BAMS-87-3-343.

Nakanishi, M., and H. Niino (2006), An improved Mellor-Yamada Level-3 model: Its numerical stability and application to a regional prediction of advection fog, *Bound.-Lay. Meteorol.*, *119*, 397–407.

Nassar, R., et al. (2008), Validation of Tropospheric Emission Spectrometer (TES) nadir ozone profiles using ozonesonde measurements, *J. Geophys. Res.*, *113*, D15S17, doi:10.1029/2007JD008819.

National Research Council (2009), Global sources of local pollution—An assessment of long-range transport of key air pollutants to and from the United States, 35–66, http://books.nap.edu/openbook.php?record_id=12743&page=35.

Neuman, J. A., et al. (2012), Observations of ozone transport from the free troposphere to the Los Angeles basin, *J. Geophys. Res.*, *117*, D00V09, doi:10.1029/2011JD016919.

Oltmans, S. J., A. S. Lefohn, J. M. Harris, and D. S. Shadwick (2008), Background ozone levels of air entering the West Coast of the U.S. and assessment of longer-term changes, *Atmos. Environ.*, *42*, 6020–6038, doi:10.1016/j.atmosenv.2008.03.034.

Parrish, D. D., J. S. Holloway, R. Jakoubek, M. Trainer, T. B. Ryerson, G. Hübler, F. C. Fehsenfeld, J. L. Moody, and O. R. Cooper (2000), Mixing of anthropogenic pollution with stratospheric ozone: A case study

from the North Atlantic wintertime troposphere, *J. Geophys. Res.*, *105*(D19), 24,363–24,374, doi:10.1029/2000JD900291.

Parrish, D. D., K. C. Aikin, S. J. Oltmans, B. J. Johnson, M. Ives, and C. Sweeny (2010), Impact of transported background ozone inflow on summertime air quality in a California ozone exceedance area, *Atmos. Chem. Phys.*, *10*, 10,093–10,109, doi:10.5194/acp-10-10093-2010.

Pfister, G. G., et al. (2011), Characterizing summertime chemical boundary conditions for air masses entering the US West Coast, *Atmos. Chem. Phys.*, *1769–1790*, doi:10.5194/Acp-11-1769-2011.

Pierce, R. B. (2011), Chemical and aerosol data assimilation activities during CalNex, CalNex data workshop, http://www.arb.ca.gov/research/calnex2010/da_workshop_may2011/tuesday/calnex_data_workshop_pierce_final.pdf.

Pierce, R. B., et al. (2007), Chemical data assimilation estimates of continental U.S. ozone and nitrogen budgets during the Intercontinental Chemical Transport Experiment–North America, *J. Geophys. Res.*, *112*, D12S21, doi:10.1029/2006JD007722.

Pommier, M., C. A. McLinden, and M. Deeter (2013), Relative changes in CO emissions over megacities based on observations from space, *Geophys. Res. Lett.*, *40*, 3766–3771, doi:10.1002/grl.50704.

Richards, N. A. D., G. B. Osterman, E. V. Browell, J. W. Hair, M. Avery, and Q. Li (2008), Validation of Tropospheric Emission Spectrometer ozone profiles with aircraft observations during the Intercontinental Chemical Transport Experiment–B, *J. Geophys. Res.*, *113*, D16S29, doi:10.1029/2007JD008815.

Russell, A. R., L. C. Valin, and R. C. Cohen (2012), Trends in OMI NO_2 observations over the United States: Effects of emission control technology and the economic recession, *Atmos. Chem. Phys.*, *12*, 12,197–12,209, doi:10.5194/acp-12-12197-2012.

Ryerson, T. B., et al. (2013), The 2010 California Research at the Nexus of Air Quality and Climate Change (CalNex) field study, *J. Geophys. Res. Atmospheres*, *118*, 5830–5866, doi:10.1002/jgrd.50331.

Saide, P. E., G. R. Carmichael, S. N. Spak, L. Gallardo, A. E. Osses, M. A. Mena-Carrasco, and M. Pagowski (2011), Forecasting urban PM_{10} and $PM_{2.5}$ pollution episodes in very stable nocturnal conditions and complex terrain using WRF-Chem CO tracer model, *Atmos. Environ.*, *45*(16), 2769–2780, doi:10.1016/j.atmosenv.2011.02.001.

Sandu, A., D. N. Daescu, G. R. Carmichael, and T. Chai (2005), Adjoint sensitivity analysis of regional air quality models, *J. Comput. Phys.*, *204*(1), 222–252.

Skamarock, W. C., J. B. Klemp, J. Dudhia, D. O. Gill, D. M. Barker, W. Wang, and J. G. Powers (2008), A description of the Advanced Research WRF Version 3, www.mmm.ucar.edu/wrf/users/docs/arw v3.pdf.

Smith, K. R., et al. (2009), Public health benefits of strategies to reduce greenhouse-gas emissions: Health implications of short-lived greenhouse pollutants, *Lancet*, *374*(9707), doi:10.1016/S0140-6736(09)61716-5.

Steiner, A. L., S. Tonse, R. C. Cohen, A. H. Goldstein, and R. A. Harley (2006), Influence of future climate and emissions on regional air quality in California, *J. Geophys. Res.*, *111*, D18303, doi:10.1029/2005JD006935.

Stith, J. L., et al. (2009), An overview of aircraft observations from the Pacific dust experiment campaign, *J. Geophys. Res.*, *114*, D05207, doi:10.1029/2008JD010924.

Tang, Y., et al. (2004), Multiscale simulations of tropospheric chemistry in the eastern Pacific and on the U.S. West Coast during spring 2002, *J. Geophys. Res.*, *109*, D23S11, doi:10.1029/2004JD004513.

Tang, Y. H., et al. (2007), Influence of lateral and top boundary conditions on regional air quality prediction: A multiscale study coupling regional and global chemical transport models, *J. Geophys. Res.*, *112*, D10S18, doi:10.1029/2006JD007515.

Task Force on Hemispheric Transport of Air Pollution (TF HTAP) (2010), 2010 final assessment report, part A: Ozone and particulate matter, http://www.htap.org/activities/2010_Final_Report/HTAP%202010%20Part%20A%20110407.pdf.

TES Level 3 Algorithms, Requirements and Products, version 2.0 (2005), http://tes.jpl.nasa.gov/uploadedfiles/Level3_v2.0.pdf, accessed in September 2013.

Tong, D. Q., and D. L. Mauzerall (2008), Summertime state-level source-receptor relationships between nitrogen oxide emissions and downwind surface ozone concentrations over the continental United States, *Environ. Sci. Tech.*, doi:10.1021/es7027636.

U.S. Census Bureau 2010 (2011), http://factfinder2.census.gov/faces/nav/jsf/pages/index.xhtml, accessed in April 2013.

U.S. Environmental Protection Agency (2010), Fact sheet: Proposal to revise the national ambient air quality standards for ozone, http://www.epa.gov/air/ozonepollution/pdfs/fs20100106std.pdf.

U.S. Geological Survey (2001), http://egsc.usgs.gov/isb/pubs/booklets/elvadist/elvadist.html, accessed in 2013.

Wallace, J. M., and D. S. Gutzler (1981), Teleconnections in the geopotential height field during the Northern Hemisphere winter, *Mon. Weather Rev.*, *109*, 784–812.

Wiedinmyer, C., S. K. Akagi, R. J. Yokelson, L. K. Emmons, J. A. Al-Saadi, J. J. Orlando, and A. J. Soja (2011), The Fire Inventory from NCAR (FINN): A high resolution global model to estimate the emissions from open burning, *Geosci. Model Dev.*, *4*, 625–641, doi:10.5194/gmd-4-625-2011.

Wild, O., et al. (2012), Modelling future changes in surface ozone: A parameterized approach, *Atmos. Chem. Phys.*, *12*, 2037–2054, doi:10.5194/acp-12-2037-2012.

Worden, J., X. Liu, K. Bowman, K. Chance, R. Beer, A. Eldering, M. Gunson, and H. Worden (2007), Improved tropospheric ozone profile retrievals using OMI and TES radiances, *Geophys. Res. Lett.*, *34*, L01809, doi:10.1029/2006GL027806.

Worden, H. M., Y. Cheng, G. Pfister, G. R. Carmichael, Q. Zhang, D. G. Streets, M. Deeter, D. P. Edwards, J. C. Gille, and J. R. Worden (2012), Satellite based estimates of reduced CO and CO_2 emissions due to traffic restrictions during the 2008 Beijing Olympics, *Geophys. Res. Lett.*, *39*, L14802, doi:10.1029/2012GL052395.

Worden, H. M., et al. (2013), Decadal record of satellite carbon monoxide observations, *Atmos. Chem. Phys.*, *13*, 837–850, doi:10.5194/acp-13-837-2013.

Yu, M., G. R. Carmichael, T. Zhu, and Y. Cheng (2012), Sensitivity of predicted pollutant levels to urbanization in China, *Atmos. Environ.*, *60*, 544–554, doi:10.1016/j.atmosenv.2012.06.075.

Yver, C. E., H. D. Graven, D. D. Lucas, P. J. Cameron-Smith, R. F. Keeling, and R. F. Weiss (2013), Evaluating transport in the WRF model along the California coast, *Atmos. Chem. Phys.*, *13*, 1837–1852, doi:10.5194/acp-13-1837-2013.

Zhang, L., J. D. Jacob, N. V. Downey, D. A. Wood, D. Blewitt, C. C. Carouge, A. van Donkelaar, D. B. A. Jones, L. T. Murray, and Y. Wang (2011), Improved estimate of the policy-relevant background ozone in the United States using the GEOS-Chem global model with 1/2 degrees 2/3 degrees horizontal resolution over North America, *Atmos. Environ.*, *45*, 6769–6776, doi:10.1016/j.atmosenv.2011.07.054.